The Oxygen Valve on Hydrogen Escape Since the Great Oxidation Event

Gregory Cooke[1], Dan Marsh[2], Catherine Walsh[2], Felix Sainsbury-Martinez[2], and Marrick Braam[3]

[1]Institute of Astronomy, University of Cambridge, CB3 0HA, UK.
[2]School of Physics and Astronomy, University of Leeds, Leeds, LS2 9JT, UK.
[3]Center for Space and Habitability, University of Bern, Gesellschaftsstrasse 6, 3012 Bern, Switzerland.

Correspondence: Gregory Cooke (gjc53@cam.ac.uk), Catherine Walsh (c.walsh1@leeds.ac.uk)

Abstract. The Great Oxidation Event (GOE) was a 200 Myr transition circa 2.4 billion years ago that converted the Earth's anoxic atmosphere to one where molecular oxygen (O_2) was abundant (volume mixing ratio $> 10^{-4}$). This significant rise in O_2 is thought to have substantially throttled hydrogen (H) escape and the associated water (H_2O) loss. Atmospheric estimations from the GOE onward place O_2 concentrations ranging between 0.1% to 150% PAL, where PAL is the present atmospheric level of 21% by volume. In this study we use WACCM6, a three-dimensional Earth System Model to simulate Earth's atmosphere and predict the diffusion-limited escape rate of hydrogen due to varying O_2 post-GOE. We find that O_2 indirectly acts as a control valve on the amount of hydrogen atoms reaching the homopause in the simulations: less O_2 leads to decreased O_3 densities that reduce local tropical tropopause temperatures by up to 17 K, which increases H_2O freeze-drying and thus reduces the primary source of hydrogen in the considered scenarios. The maximum differences between all simulations in the total H mixing ratio at the homopause and the associated diffusion-limited escape rates are a factor of 3.2 and 4.7, respectively. The prescribed CH_4 mixing ratio (0.8 ppmv) sets a minimum diffusion escape rate of $\approx 2 \times 10^{10}$ mol H yr^{-1}, effectively a negligible rate when compared to pre-GOE estimates ($\sim 10^{12} - 10^{13}$ mol H yr^{-1}). Because the changes in our predicted escape rates are comparatively minor, our numerical predictions support geological evidence that the majority of Earth's hydrogen escape occurred prior to the GOE. Our work demonstrates that estimations of how the tropical tropopause layer and the associated hydrogen escape rate evolved through Earth's history requires 3D chemistry-climate models which include a global treatment of water vapour microphysics.

1 Introduction

A key component of Earth's atmospheric and biological history is its water (H_2O). The relative amount of H_2O that was present during the Earth's formation versus the quantity delivered by volatile-rich bodies (e.g., comets and asteroids; Dauphas et al., 2000; Izidoro et al., 2013), as well as the H_2O lost to space through hydrogen escape (Catling et al., 2001; Genda and Ikoma, 2008), or exchanged into the interior (Hallis et al., 2015; Korenaga et al., 2017), has had an important impact on how the Earth's surface and the atmosphere have developed. Beyond Earth, the solar system's terrestrial planet atmospheres are desiccated and consequently, Venus and Mars are both apparently desolate environments. It's possible that Venus was never habitable (Turbet et al., 2021; Warren and Kite, 2023; Constantinou et al., 2024), but Mars was likely habitable early in its history before its

water was isolated to the subsurface and the crust (di Achille and Hynek, 2010; Orosei et al., 2018; Scheller et al., 2021; Lauro et al., 2021; Sauterey et al., 2022; Zheng et al., 2024; Wright et al., 2024). Venus is now too hot for liquid H_2O to persist and probably lost much of its natal H_2O through atmospheric hydrogen escape (Ingersoll, 1969; Kulikov et al., 2006; Kane et al., 2019; Cangi et al., 2024; Gu et al., 2025).

In contrast, Earth has mostly remained temperate throughout its history, with liquid water persisting on the surface for over 4 billion years (Feulner, 2012, and references therein), although there were periods of widespread glaciation at either end of the Proterozoic eon (2.4 – 0.541 Gyr ago; Young, 2013; Warke et al., 2020). A mostly temperate Earth has been possible despite a fainter Sun in Earth's past (Bahcall et al., 2001; Feulner, 2012; Charnay et al., 2020), in combination with fluctuations in albedo (Charnay et al., 2020; Goldblatt et al., 2021) and atmospheric composition, in particular the greenhouse gases CO_2 (Sheldon, 2006, 2013; Kanzaki and Murakami, 2015) and CH_4 (Daines and Lenton, 2016; Zhao et al., 2018; Laakso and Schrag, 2019; Fakhraee et al., 2019). Geochemical proxies suggest a broad range but generally greater past abundance for CO_2, whereas only loose constraints have been placed on CH_4 (Catling and Zahnle, 2020, and references therein), with debates regarding whether CH_4 during the Proterozoic was higher or lower in abundance than present day still ongoing (see Discussion section).

As all known life requires liquid H_2O, the history of Earth's H_2O is inextricably tied to the evolution of Earth's life. From isotopic evidence and computational modelling, since its formation, the Earth may have lost between 0.13 and 2 times the present ocean volume (Pope et al., 2012; Kurokawa et al., 2018; Zahnle et al., 2019). Indeed, the early Archean Earth (4 – 2.4 Gyr ago), before 3.2 Gyr ago, may have been fully covered in a global ocean (Dong et al., 2021). The current hydrogen escape rate is $\approx 4 \times 10^{10}$ mol of H yr^{-1}, corresponding to roughly 1 metre of global water loss per 1 billion years (Zahnle et al., 2013). Given that the Earth's ocean can be up to 11 km deep (Gardner et al., 2014), and its mean depth is ≈ 3.6 km (Charette and Smith, 2010), the loss rate is insignificant. This suggests a different past for hydrogen escape than the constant modern rate would imply.

Therefore, an important but uncertain component of Earth's water loss is determining the amount of hydrogen (H) that has escaped to space. As the lightest element, H escapes atmospheres more readily than other elements and chemical compounds. On Earth, hydrogen atoms exist in many different chemical species in the lower and middle atmosphere (Brasseur and Solomon, 2005). The four major chemical constituents that contribute hydrogen atoms to the upper atmosphere, and therefore the species we focus on in this work, are H, H_2, H_2O, and CH_4. Atmospheric escape of hydrogen can occur from a planet through several mechanisms, including: Jeans escape, hydrodynamic flow, sputtering, impacts, photochemical escape, and charge exchange escape (Lundin et al., 2007; Johnson, 2010; Shematovich and Marov, 2018; Gronoff et al., 2020). For these mechanisms, with the exception of impacts and hydrodynamic flow, the hydrogen escapes from the exosphere at the top of the atmosphere. In such cases, hydrogen cannot escape faster than it can be delivered to the exosphere through molecular diffusion. This is known as 'diffusion-limited hydrogen escape' (Hunten, 1973; Hunten and Donahue, 1976; Walker, 1977; Kasting and Catling, 2003; Zahnle et al., 2013). The diffusion-limited rate of hydrogen escape is set by two controlling bottlenecks, the upward diffusion of hydrogen atoms (mostly in H_2O and CH_4) through the tropopause 'cold trap', and the upward diffusion of hydrogen atoms through molecular diffusion above the homopause[1] (Catling et al., 2001; Catling and Kasting, 2017).

[1]The homopause is the atmospheric point above which molecular diffusion dominates and below which turbulent diffusion dominates

The primary hydrogen bottleneck, the cold trap, is where the saturation mixing ratio of H_2O and ice is at a minimum, such that it modulates the amount of H_2O propagating upwards into the stratosphere (Kasting et al., 2015). On Earth, the cold trap is typically described as the tropical tropopause layer (TTL). The TTL is three-dimensional and is defined as the transition region between the Hadley circulation in the troposphere and the start of the deep branch of the Brewer-Dobson circulation (Brasseur and Solomon, 2005; Fueglistaler et al., 2009; Glanville and Birner, 2017). Despite being located above the tropics (at 12 – 16 km in altitude, which is 70 – 150 hPa in pressure), which have on average greater surface temperatures than higher latitudes, the TTL is defined by its cold temperatures (Brasseur and Solomon, 2005; Fueglistaler et al., 2009). The cause of this is adiabatic cooling as air is transported upwards from the convective troposphere into the stratosphere, and this cold temperature region leads to the removal of water vapor from the atmosphere through condensation (Brewer, 1949; Newell and Gould-Stewart, 1981; Danielsen, 1982; Pommereau and Held, 2007). The location, temperatures, and dynamics of the TTL are affected by seasons (Kim and Son, 2012) and climate change (Randel and Jensen, 2013; Lin et al., 2017; Zou et al., 2023; Zolghadrshojaee et al., 2024). Of the major H-bearing species, only H_2O is significantly affected by temperatures in the TTL, whereas H_2 and CH_4, which don't condense in Earth's atmosphere, are unaffected by the cold trap mechanism.

In the stratosphere, hydrogen atoms are interchanged between CH_4, H_2O and H_2, until reaching the homopause (Catling and Kasting, 2017). At altitudes exceeding the homopause, through diffusive separation, the lighter atmospheric constituents with lower molecular masses increase in relative abundance with decreasing pressure (e.g., H, He, O, and N). Note that H_2 would also increase but it is rapidly photodissociated into H. Hence, above the homopause, H dominates the total hydrogen budget (Catling and Kasting, 2017).

The atmosphere of the Archean Earth was likely weakly reducing with greater quantities of CH_4, CO, and H_2 (Kasting et al., 2001; Kharecha et al., 2005; Kadoya and Catling, 2019; Catling and Zahnle, 2020). Midway through Earth's history, approximately 2.4 billion years ago, a rise in oxygen known as the Great Oxidation Event (GOE; Farquhar et al., 2000; Holland, 2002; Hodgskiss et al., 2019; Warke et al., 2020; Goldblatt et al., 2021) has been proposed to have significantly reduced hydrogen escape from $\sim 10^{12} - 10^{13}$ mol H yr^{-1} to $\sim 10^{10}$ mol H yr^{-1} (Catling et al., 2001; Zahnle et al., 2013). This is because an oxygenated atmosphere destroys reducing species (e.g., H_2 and CH_4), resulting in lower amounts of such gases which contribute hydrogen atoms to the upper atmosphere.

In conjunction, atmospheric escape of hydrogen may have played a significant role in shaping Earth's atmosphere through time. It is thought to at least be partially responsible for oxidising the Earth's surface: when H_2O is photodissociated above the troposphere, the liberated hydrogen (H) can escape to space, and the oxygen (O) left behind oxidises the Earth (Catling et al., 2001; Claire et al., 2006; Zahnle et al., 2013). Alongside photosynthetic production of O_2 from cyanobacteria, this process is hypothesized to have contributed to the occurrence of the GOE because the process of hydrogen escape and subsequent oxidation is irreversible, leading to a reduced sink of O_2 over time (Catling et al., 2001; Claire et al., 2006; Zahnle et al., 2013). Nevertheless, considerable uncertainty persists regarding the precise temporal evolution of Earth's atmosphere (Kasting, 2025), with hydrogen escape a key aspect of the holistic picture.

There is no direct way to determine the amount of hydrogen that has escaped in Earth's history. As mentioned, several measurements can be used to infer this quantity, and the chronology of one of the heaviest gases, Xe, may be informative.

Xe is more easily ionised compared to the other noble gases which do not exhibit the same fractionation (the so-called Xenon paradox; Anders and Owen, 1977; Zhu et al., 2013). It was proposed that Xe^+ could escape Earth's atmosphere when propelled by H^+ ions, and this has been shown to be a feasible physical process (Zahnle et al., 2019). Accordingly, the timing of Earth's Xe fractionation (see figure 3 in Zahnle et al., 2019) may trace high levels of atmospheric hydrogen escape during the Archean eon. There has been relatively small changes in Xe fractionation since the GOE (Avice et al., 2018), indicating the vast majority of historical hydrogen escape occurred prior to this time (i.e., before ~ 2.4 Gyr ago).

Whilst hydrogen escape rates may have been much lower in the last ~ 2.4 Gyr, to our knowledge, no work has quantitatively estimated escape rates since the GOE occurred using a 3D model. In this work, we build upon a previous study (Cooke et al., 2022) which simulated a range of O_2 concentrations that may have been present on the Earth for the last 2.4 Gyr and found that lower O_3 columns were predicted compared to previous work (Kasting and Catling, 2003; Segura et al., 2003; Rugheimer et al., 2015; Rugheimer and Kaltenegger, 2018; Kaltenegger et al., 2020; Ji et al., 2023). More recent work has in part supported the results of lower O_3 for a given O_2 mixing ratio (Yassin Jaziri et al., 2022; Ji et al., 2024; Liu et al., 2025). O_3 and its associated UV heating is responsible for the temperature inversion that creates the Earth's stratosphere, and this heating affects the temperatures in the TTL. Therefore, the O_2 fluctuations following the GOE may have modulated the upward transport of H_2O through the TTL and consequently, hydrogen escape too.

Using the 3D chemistry-climate model WACCM6, we first explore the affect of changing the O_2 abundance on the TTL region, before investigating the influence it may have had on hydrogen escape during the Proterozoic eon. Our aim is to estimate how changes to atmospheric O_2 alone can affect the diffusion-limited hydrogen escape rate. In terms of hydrogen escape fluctuations, our focus is on H_2O, and we hold the mixing ratios of H_2 and CH_4 constant at the surface. We note that CO_2, CH_4 and H_2 are likely to have varied during the past 2.4 billion years (Catling and Zahnle, 2020), as will have the luminosity of the Sun (Feulner, 2012). These variables are important because CH_4 and H_2 are key hydrogen carriers to the upper atmosphere, and additionally CH_4 and CO_2 provide greenhouse warming which can affect TTL temperatures. The TTL will also have been affected from the reduced total insolation from a younger Sun which would act to cool the troposphere. The purpose of this work is, however, to present the mechanism by which O_2 affects hydrogen escape. We calculate such H escape deviations, paving the way for future work on the topic to investigate other physical, chemical, and biological influences.

2 Numerical methods

2.1 WACCM6 model

The simulations we analyse are those from Cooke et al. (2022), where the Earth System Model WACCM6 (Gettelman et al., 2019) was employed to model different oxygenation levels. WACCM6 is a configuration of the Coupled Earth System Model (CESM), and we use version 2.1.3 (CESM2.1.3[2]) with minor code alterations in the initial conditions[3], which we describe in this section.

[2]https://www.cesm.ucar.edu/models/cesm2

[3]ExoCESM GitHub: https://github.com/exo-cesm/CESM2.1.3/tree/main/O2_Earth_analogues

The first simulation we perform commences with initial conditions which are intended to be representative of Earth's pre-industrial (PI) atmosphere circa 1850, alongside contemporary ocean and land settings, and the current orbital setup with a 23.4° obliquity and 24-hour rotation rate. Deep time paleoclimate studies would often change the continents and we accept that this is a limitation with the WACCM6 model where continents cannot currently be modified. The circulation pattern and climate would have been different in the past due to various factors, which include the younger Sun, different greenhouse gas concentration, and the formation and break up of supercontinents such as Pangea and Columbia/Nuna (Rogers and Santosh, 2002; Feulner, 2012; Fiorella and Sheldon, 2017; Catling and Zahnle, 2020). The model's spatial resolution for the atmosphere was set at 1.875° latitude by 2.5° longitude (yielding a 96×144 horizontal grid). This configuration utilizes 70 atmospheric layers in vertical pressure coordinates extending from the surface (approximately 1000 hPa) to the thermosphere (4.5×10^{-6} hPa, or ~ 150 km). The land component (CLM5.0) operates on the same $1.9^\circ \times 2.5^\circ$ horizontal grid as the atmosphere to maintain consistency in surface flux exchanges. The simulation employs an interactive ocean via the POP2 model, which operates on a 1° displaced-pole grid. This ocean grid features 320×384 points, with enhanced latitudinal resolution near the equator to better resolve tropical dynamics. This same grid is utilized by the Sea-Ice (CICE5) and Wave (WaveWatch3) components. Additionally, freshwater discharge is included in the MOSART river transport model on a 0.5° global grid.

Both atmospheric and oceanic components of the model are interactive, allowing dynamic responses to environmental stimuli like temperature changes. Our simulations incorporated middle atmosphere chemistry as described by Emmons et al. (2020), featuring 98 chemical species and 298 reactions, including O_3 chemistry. The atmospheric time step, Δt, was set at 30 minutes. The concentrations of 75 species were computed using an implicit numerical scheme, while 22 long-lived species were computed using an explicit numerical scheme (Sandu et al., 1997; Brasseur and Solomon, 2005). N_2 is considered invariant. Absorption of light by CO_2 and H_2O in the Schumann-Runge (S-R bands) is not included in these simulations, and neither is scattering at wavelengths < 200 nm. For more details on the inclusion of these processes, we refer the reader to Ji et al. (2023) and Ji et al. (2024), as well as Section 4.2 where we discuss how it might impact our results.

In total, eight simulations were performed for the Earth system with different mixing ratios of atmospheric O_2, where the atmospheric pressure was kept the same by changing the abundance of the background gas, N_2. O_2 mixing ratios are given in terms of present atmospheric level (PAL), which is 21% by volume. The O_2 surface mixing ratios span values between 0.1 – 150% PAL, which are within estimates for the Earth over the last 2.4 billion years (Lyons et al., 2014; Large et al., 2019; Catling and Zahnle, 2020; Steadman et al., 2020). These temporal estimates do not always agree, so we remain agnostic and perform simulations covering the whole range. The simulation names are PI, 150% PAL, 50% PAL, 10% PAL, 5% PAL, 1% PAL, 0.5% PAL, and 0.1% PAL. CO_2, CH_4, N_2O, and H_2, were held fixed at values of 284 ppmv, 0.8 ppmv, 273 ppbv, and 0.5 ppmv, respectively. The mixing ratios or fluxes of gases specified at the surface were kept constant as O_2 was altered. This assumption is likely not realistic for the entirety of the last 2.4 Gyr, but it allows us to isolate the role O_2 changes make to the chemistry and dynamics of the atmosphere. Water vapor feedback, in terms of evaporation and rainout, is included in WACCM6, but hydrogen escape and water loss are not explicitly simulated. Instead, we estimate these values once quasi-steady state has been reached in the simulation (see section 2.2).

We average the outputs of the WACCM6 simulations over the last four years of the simulation once the middle atmospheric (defined here as between 12 – 100 km in altitude; Brasseur and Solomon, 2005) trend in total hydrogen atoms has halted, and this required between 30 and 90 simulations years for the different scenarios.

2.2 Diffusion-limited hydrogen escape rate

The diffusion-limited hydrogen escape rate (Hunten, 1973; Kasting and Catling, 2003), $\Phi_{\rm esc}$, is proportional to the total mixing ratio of hydrogen-bearing species, $f_{\rm T}({\rm H})$, at the homopause:

$$\Phi_{\rm esc} \propto f_{\rm T}({\rm H}), \tag{1}$$

where $f_{\rm T}({\rm H})$, can be written as

$$f_{\rm T}({\rm H}) = f({\rm H}) + 2f({\rm H_2}) + 2f({\rm H_2O}) + 4f({\rm CH_4})..., \tag{2}$$

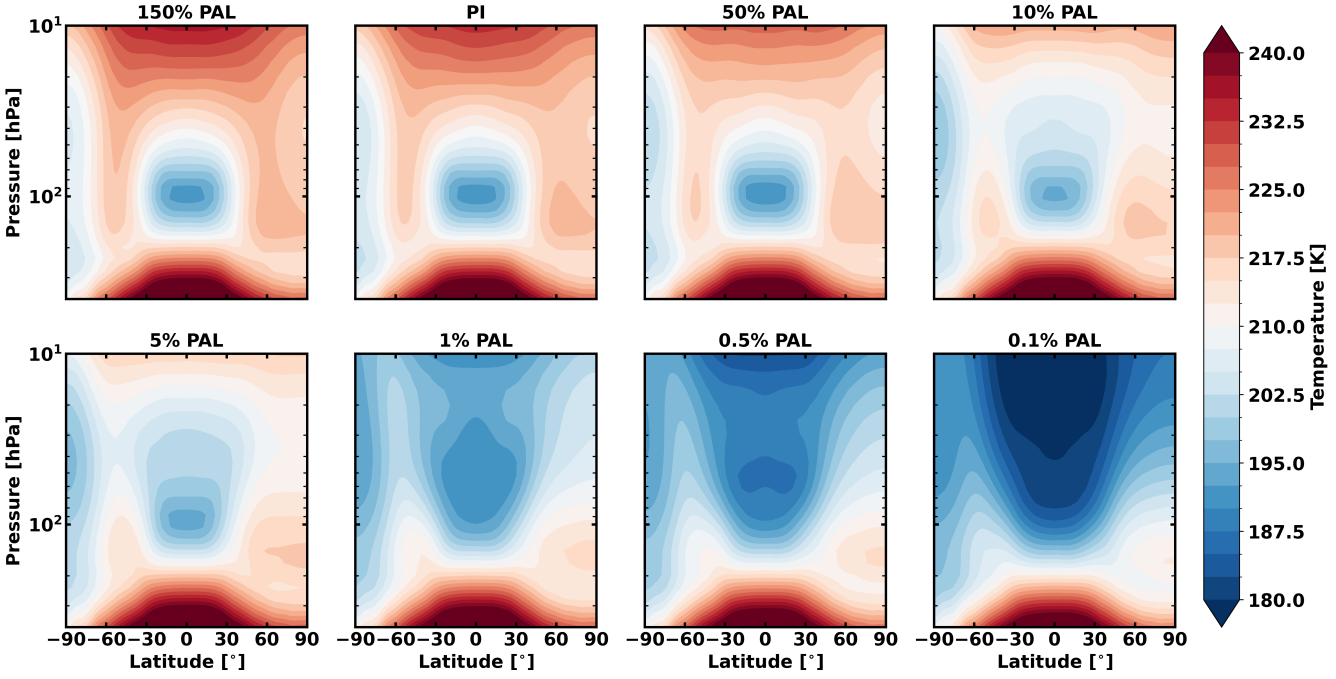

Figure 1. The zonal mean of atmospheric temperature (in K) is shown for simulations with O_2 mixing ratios between 150% PAL and 0.1% PAL, where O_2 decreases in abundance from the top left panel to the bottom right panel. The colour bar shows hotter temperatures in red and colder temperatures in blue. The TTL region is $\pm 23.4^\circ$ from the equator and between 70–150 hPa in pressure.

and so on, accounting for all hydrogen-bearing species. We focus on evaluating the abundances of H, H_2, H_2O, and CH_4. In modern Earth's atmosphere, at the tropopause, the H_2 and CH_4 mixing ratios are ≈ 0.55 ppmv (Catling and Kasting, 2017) and ≈ 1.9 ppmv (Saunois et al., 2025), respectively. There, the H_2O mixing ratio varies between $\approx 2.5 - 4.5$ ppmv, with a mean stratospheric entry value of $\sim 3.5 - 4$ ppmv (Fueglistaler et al., 2009; Gettelman et al., 2019). This puts the stratospheric entry value of total hydrogen at ~ 17 ppmv, although with CH_4 at a lower concentration during the pre-industrial period, the entry value would be closer to ~ 12 ppmv. In our simulations, the lower boundary mixing ratios are instead mixing ratios of 0.5 ppmv and 0.8 ppmv for H_2 and CH_4, respectively, corresponding to pre-industrial values. Consequently, H_2O is the primary carrier of hydrogen atoms to the middle atmosphere. Other H-bearing species such as OH, HO_2, and H_2O_2 are included in the WACCM6 model but are not sufficiently abundant to contribute significantly to the overall hydrogen budget.

The calculation of Φ_{esc} at the homopause can be made by considering the binary diffusion coefficients which depend on the temperature of the atmosphere and the chemical species. Φ_{esc}, in units of atoms cm^{-2} s^{-1}, is given by

$$\Phi_{\text{esc}} = \sum_{i=1}^{n} \frac{N_i f(i) b_i}{H_h}, \tag{3}$$

where H_h is the atmospheric scale height at the homopause, N_i is the number of hydrogen atoms in each chemical species, i, and b_{i} is the binary diffusion parameter for each constituent. The binary diffusion coefficient depends on the temperature of the atmosphere at the homopause (T_h), the masses of the species, and their collision cross-sections. For each species considered here, the binary diffusion coefficients are $b_{\text{H}} = 6.5 \times 10^{17} T_h^{0.7}$, $b_{\text{H}_2} = 2.67 \times 10^{17} T_h^{0.75}$, $b_{\text{H}_2\text{O}} = 0.137 \times 10^{17} T_h^{1.072}$, $b_{\text{CH}_4} = 0.734 \times 10^{17} T_h^{0.750}$. These binary diffusion parameters for H, H_2, and H_2O are sourced from Hunten (1973) and CH_4 is sourced from Banks and Kockarts (1973). The calculations are made for the whole atmosphere (latitude and longitude at the homopause) before calculating a longitudinally-averaged and latitudinally-weighted mean.

From Earth's exosphere, hydrogen escapes faster than it is delivered, such that throughout this work, we will assume that the loss rate of hydrogen atoms is diffusion-limited (ignoring hydrodynamic escape and impacts). Note that it is possible for hydrogen to escape slower than this upper limit, provided the rate of loss from the exosphere is the limiting factor (e.g., energy-limited escape, photon-limited escape; Tian et al., 2005; Salz et al., 2016; Owen and Alvarez, 2016; Lehmer and Catling, 2017).

3 Results

As part of the hydrological cycle, liquid water evaporates from the surface and warm, moist air rises due to buoyancy. Hence, rivers, lakes, and predominantly the ocean, act as a sources of hydrogen atoms to the atmosphere. We will present the results in terms of how the total hydrogen mixing ratio starts at the surface and how it changes with decreasing atmospheric pressure (increasing altitude). This includes tracking the proportion of hydrogen atoms bound in different species, such as H_2O and CH_4. We will show how the O_2 mixing ratio affects the total hydrogen mixing ratio through the atmosphere and ultimately the amount of hydrogen atoms diffusing up to the exosphere. In the following subsection, we consider how O_2 affects clouds,

condensation, and the cold trap at the top of the troposphere. These processes act to keep hydrogen atoms in the troposphere that would otherwise mix into the stratosphere and upwards to eventually escape to space.

3.1 Water vapour through the cold trap

In every simulation, the global mean mixing ratio of each species at the surface for H_2O, H, CH_4, and H_2, is $\sim 10,000$ ppmv, $< 10^{-8}$ ppmv, ≈ 0.8 ppmv, and ≈ 0.5 ppmv respectively, with the latter two molecules specified with fixed mixing ratios at the surface. As temperature and pressure decline with altitude in the troposphere, the atmosphere cannot hold as much H_2O vapor. This is because the drop in pressure causes the air to cool (adiabatic cooling), and the saturation vapor pressure of water, which determines the air's capacity for water vapor, is strongly dependent on temperature. Fig. 1 presents the zonal mean (averaged over longitude) of the atmospheric temperature between the surface and 10 hPa (~ 30 km in altitude) for all the WACCM6 simulations. The temperature structure of the atmosphere is set by the strength and spectral shape of the incoming radiation, the moist adiabat in the troposphere, atmospheric composition (providing heating and cooling in different layers), clouds and ice, and atmospheric dynamics. Between 150% PAL and 50% PAL, the temperature structure at pressures greater than 10 hPa (or altitudes below 10 hPa) is similar. At 10% and 5% PAL, the temperature increases in the middle atmosphere, and this is noticeable in the tropics between 200 – 30 hPa and at northern $(45 - 90°)$ latitudes between 200 – 100 hPa. At $\leq 1\%$ PAL of O_2, the stratosphere begins to become significantly cooler, with the 10 hPa pressure level ~ 60 K cooler in the 0.1% PAL simulation compared to the 150% PAL simulation. A globally averaged stratospheric temperature inversion of ≈ 2 K and ≈ 1

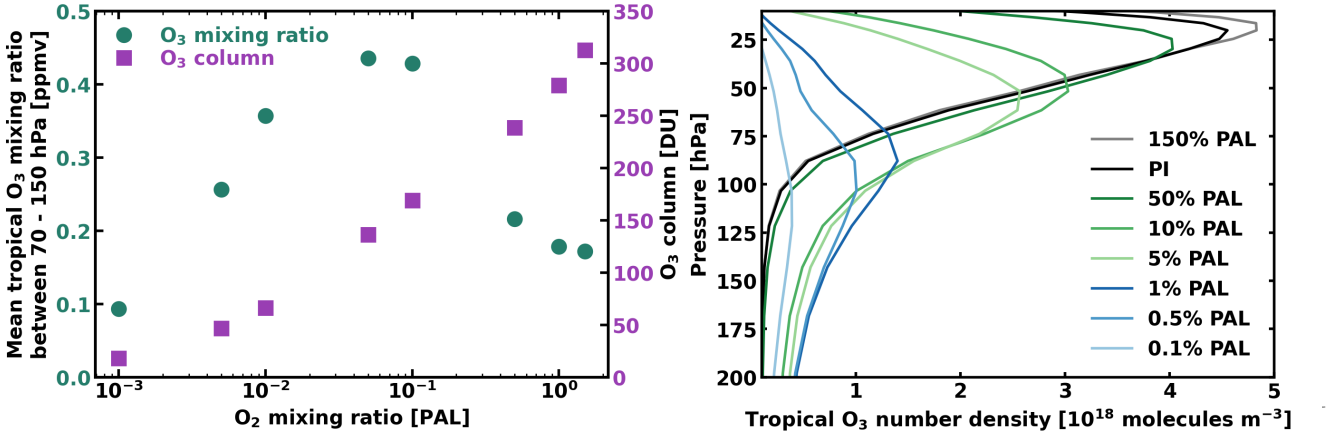

Figure 2. Left: The mean tropical (defined at latitudes $\pm 24°$ from the equator) O_3 mixing ratio between 70 – 150 hPa is plotted on the left vertical axis in teal circles against the atmospheric mixing ratio of O_2 at the surface in terms in terms of the present atmospheric level (PAL), which is 21% by volume. The total global ozone (O_3) column density in Dobson Units (DU, where 1 DU $= 2.69 \times 10^{20}$ molecules m^{-2}) is also plotted in purple squares on the right vertical axis against the atmospheric mixing ratio of O_2. **Right**: The O_3 number density is shown for all eight simulations between 10 – 200 hPa on a linear scale (note the number density does not go to zero at pressures greater than 200 hPa, see Cooke et al., 2022).

K exists in the 1% PAL and 0.1% PAL simulations, respectively, which is significantly smaller than the ≈ 60 K temperature inversion in the PI atmosphere.

Fig. 2 shows the mixing ratio of atmospheric O_2 plotted against the O_3 column density, as well as the mean O_3 mixing ratio between 70 and 150 hPa in the tropical region, accounting for the expanse of the TTL. The figure also shows the O_3 number density in the tropics between 10 and 200 hPa. Whilst the global O_3 column density increases with increasing O_2 mixing ratio, this is not the case for the O_3 mixing ratio around the TTL region: there is instead a peak at $\approx 5-10\%$ PAL. The O_3 number density also mirrors this relationship. When O_2 is decreased, O_3 accumulates lower down in the atmosphere because the wavelengths that photolyse O_2 to produce "odd oxygen" (O + O_3) are able to penetrate deeper. Consequently, for O_2 concentrations of $\leq 10\%$ PAL, O_3 maximizes in this region near the TTL. The TTL temperatures are a balance between shortwave heating and the emission and absorption of longwave radiation. Whilst this causes higher temperatures than the PI atmosphere for 5 – 10% PAL, simulations with $\leq 1\%$ PAL have resultant lower temperatures. This effect is a local TTL phenomenon; globally, the mean tropopause temperatures decrease with decreasing O_2.

These results are in line with previous O_3 depletion experiments (albeit of a much smaller magnitude) which found that reduced O_3 concentrations cooled the TTL and led to less stratospheric water vapour (Forster et al., 2007; Xie et al., 2008; Lu et al., 2021; Zhou et al., 2022). The cooling was attributed to radiative processes. Indeed, Forster et al. (2007) showed that less O_3 in the tropical lower stratosphere caused cooling that extended into the upper tropical troposphere due to reduced downward longwave radiation. Similarly, here we find that lower middle stratospheric densities of O_3 reduces the propagation of longwave radiation downwards. This mechanism is the cause of the hotter temperatures in the higher oxygenated scenarios in Fig. 1 compared to scenarios with $\leq 1\%$ PAL. This is also why there is an asymmetry in temperatures because of hemispherical asymmetries in the O_3 distribution (there is more O_3 in the northern hemisphere) as a result of the Brewer-Dobson circulation (Dobson and Harrison, 1926; Brewer, 1949; Butchart, 2014).

In Section 1, we described how H_2O moves through the TTL to get into the stratosphere on modern Earth. The cold trap mechanism is indirectly sensitive to O_2 concentrations resulting from the aforementioned difference in O_3 and hence UV heating. Due to the difference in time-averaged zonal mean TTL temperatures between the PI and 0.1% PAL simulations of up to ≈ 17 K, more H_2O is frozen out in the form of water clouds, ice, and ice clouds (e.g., cirrus clouds; Wang and Dessler, 2012) before crossing ≈ 100 hPa in the 0.1% PAL case compared to the standard PI case. Stratospheric O_3 and H_2O are greenhouse gases, and with less H_2O reaching the stratosphere as a consequence of reduced O_3, this decreases tropospheric heating (Deitrick and Goldblatt, 2023), causing a positive feedback effect, albeit a small one: there is some cooling at the surface, but this is limited to < 3 K in terms of global averaged surface temperatures.

The fractional coverage of high clouds (high clouds are defined as clouds at pressures < 400 hPa and are therefore relevant to the TTL) versus latitude is shown in Fig. 3. The coverage of high clouds for the PI, 1% PAL, and 0.1% PAL is also shown in the same figure. The O_2 mixing ratio affects high cloud coverage across the entire planet, but especially in the tropics. There is a $\approx 30\%$ increase in the peak high cloud fraction at the equator (0° latitude) from the 150% PAL simulation to the 0.1% PAL simulation, although the peak high cloud fraction for the simulations between the O_2 concentrations of 150% PAL to 1% PAL

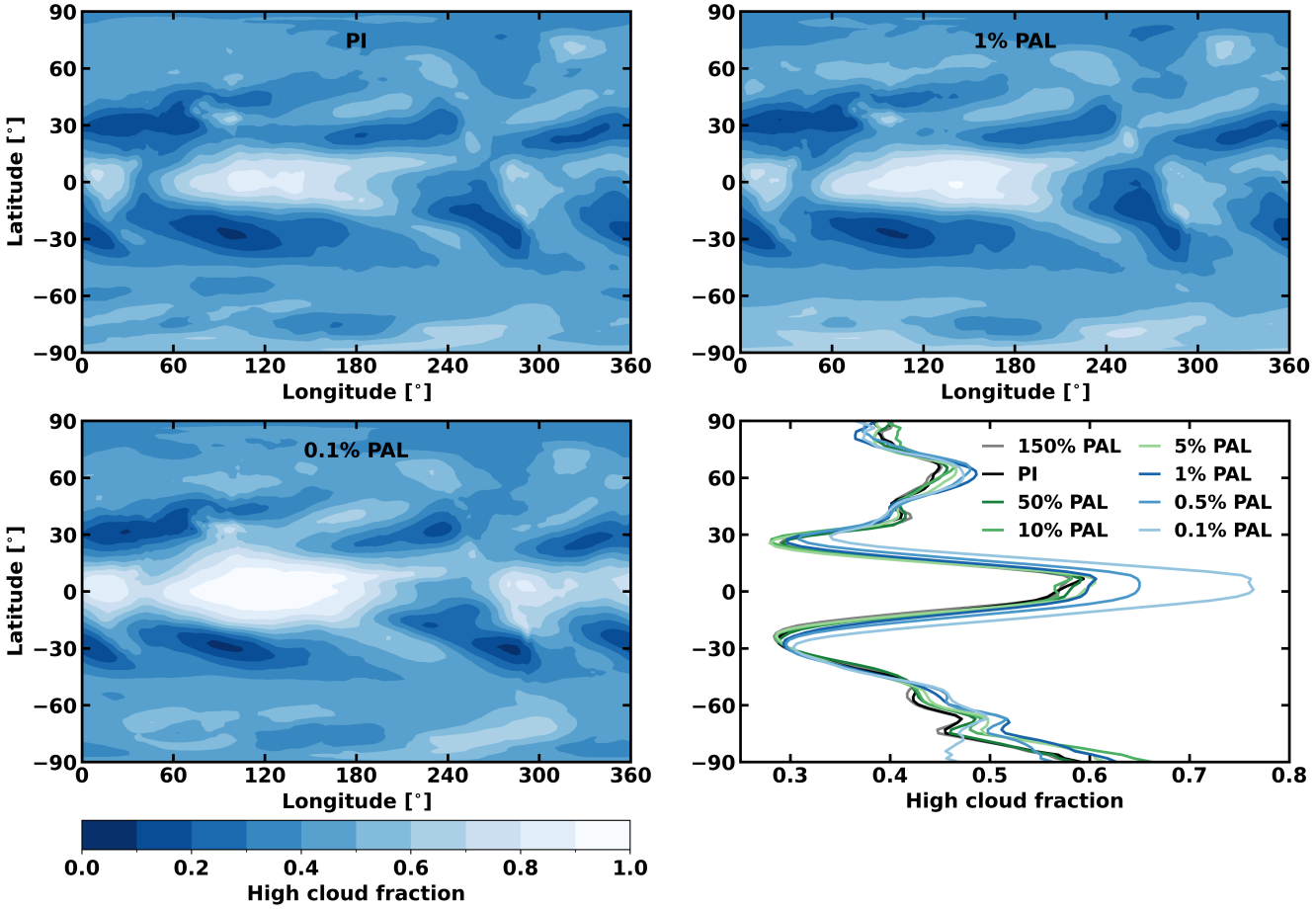

Figure 3. The **top left**, **top right**, and **bottom left** panels show the high cloud fraction as a function of longitude and latitude for the PI, 1% PAL, and 0.1% PAL scenarios, respectively. **Bottom right**: The high cloud fraction (high clouds are defined as clouds at pressures < 400 hPa) is averaged over longitude and shown as a function of latitude for all the WACCM6 simulations.

at the equator all fall within 6% of each other. Low clouds (surface – 700 hPa) and medium clouds (700 – 400 hPa) exhibit very little deviation between the simulations.

The total hydrogen mixing ratio bound in ice (ice water content and ice clouds) and H_2O for the PI and 0.1% PAL cases is shown in Fig. 4 between $-60°$ to $+60°$ latitude. At 142 hPa (roughly 14 km in altitude), the 0.1% PAL scenario has a greater amount of ice content and a lower amount of H_2O. Thus, due to the freeze-drying of the atmosphere, fewer hydrogen atoms are able to contribute to the stratospheric total hydrogen mixing ratio, $f_{\mathrm{T}}(\mathrm{H})$, when compared to the PI case. Both simulations show a larger build-up of total ice water, ice clouds, and H_2O content over the western pacific (e.g., between 90 – 150° East), as is found on modern Earth (Newell and Gould-Stewart, 1981; Dessler, 1998; Dong et al., 2020).

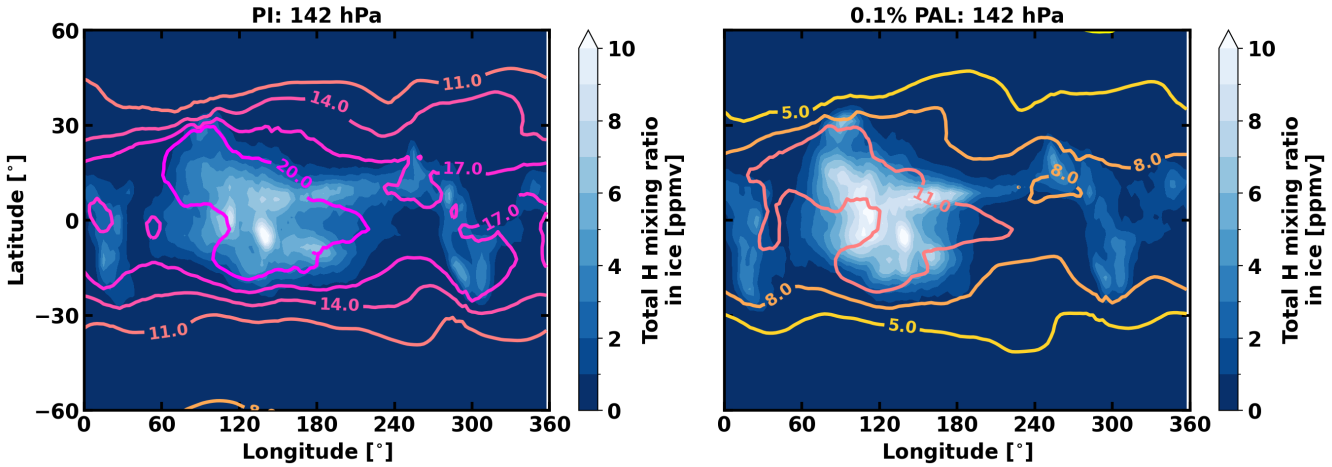

Figure 4. The atmospheric ice content (blue-white shading) and the amount of atmospheric H_2O (magenta-orange-yellow contours) is shown on the latitude-longitude grid of the Earth. Both are given in terms of ppmv. The PI simulation (**left**) and the 0.1% PAL simulation are shown (**right**). Both scenarios are shown for a pressure level of 142 hPa, which corresponds to an altitude of $\approx$ 14 km near the base of the TTL.

In the cases we have simulated, the interplay between UV radiation, O_2 mixing ratio, and 3D transport, is especially important for predicting the O_3 distribution. The amount of O_3 and the incoming UV affect temperatures around the tropopause, and ultimately how much H_2O can reach the stratosphere. Here we are exploring the impact of O_2 levels alone on the TTL temperatures and thus atmospheric escape. Other factors will have influenced TTL temperatures for the past 2.4 billion years, and these will be discussed in Section 4.

3.2 Tropical tape recorder

The tropical "tape recorder" (Mote et al., 1995; Liu et al., 2007; Glanville and Birner, 2017) for H_2O is the phenomenon where seasonal temperature fluctuations in the TTL modulate the mixing ratio of H_2O that enters the stratosphere over an annual cycle. The temperature of the TTL itself is affected by several processes, including radiative heating and cooling, deep convection, sea surface temperatures, and the Quasi-Biennial Oscillation (Fueglistaler et al., 2009; Paulik and Birner, 2012; Garfinkel et al., 2013; Tegtmeier et al., 2020). Note that the tape recorder effect exists for some other molecules too, including CO (Schoeberl et al., 2006; Liu et al., 2007; Pumphrey et al., 2008). The Brewer-Dobson circulation (Dobson and Harrison, 1926; Brewer, 1949; Butchart, 2014), over a period of months, transports H_2O upward (Glanville and Birner, 2017), causing the distinct tape recorder effect (WACCM6 is able to generate this effect - see the PI simulation in Fig. 5 and also Gettelman et al., 2019). The seasonally-varying temperatures in the TTL imprint a record on the observed mixing ratio of H_2O which is altered in the middle atmosphere in the subsequent months.

In the PI simulation, the tape recorder is easily visible over a 4-year time frame with a period of 1 year (see Fig. 5). For the PI case, the peak seasonal differences in the tape recorder effect are of order 1.5 ppmv at $\approx$ 90 hPa. Note that this amplitude is

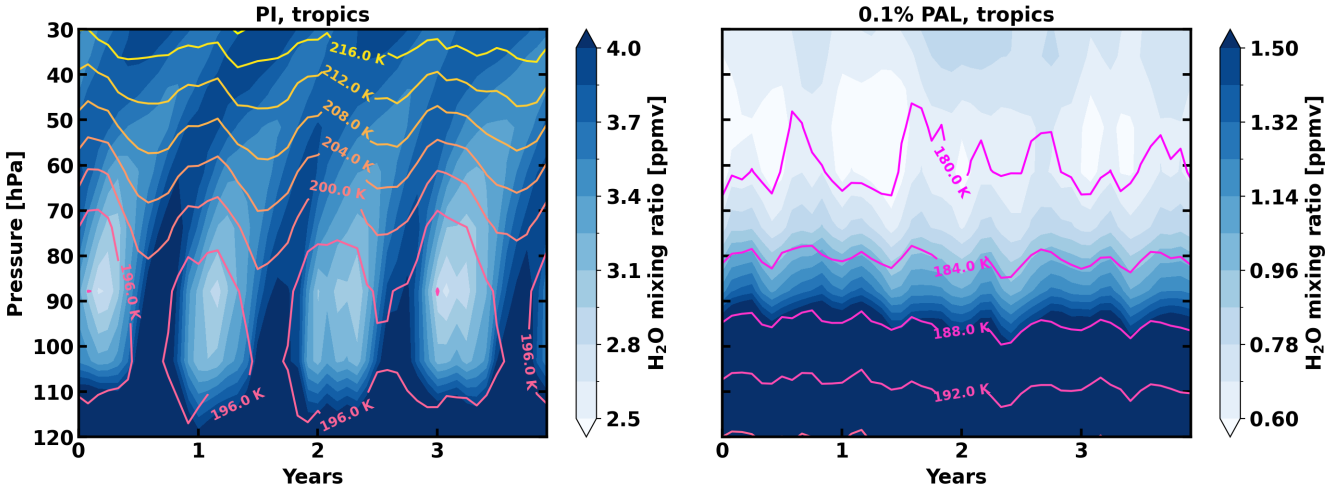

Figure 5. The water vapour mixing ratio in ppmv is shown for the PI scenario (**left**) and the 0.1% PAL scenario (**right**) between pressures of 120 – 30 hPa. Each panel shows four years in a row of each simulation, displaying the zonally averaged and latitudinally weighted H_2O mixing ratio in the tropics between $\pm 24°$. Whites show the lowest mixing ratios and darker blues show progressively larger mixing ratios. Note the different scales on each colour bar. The contours show the atmospheric temperature in kelvin, with yellow indicating higher temperatures and magenta indicating lower temperatures.

much smaller than the tape recorder variation Liu et al. (2023) found for an Earth-like exoplanet with a higher eccentricity of 0.4.

At low oxygenation states ($< 1\%$ PAL), seasonal differences in temperature and the Brewer-Dobson circulation are still present, but their magnitude is smaller so the tropical tape recorder effect is muted. Whilst the H_2O mixing ratios still vary, the tape recorder effect is no longer visible from the scale shown in Fig. 5 at 0.1% PAL because there is no clear periodic signal. Variance-preserving Fourier spectra show that the annual harmonic (1 cycle yr^{-1}) dominates the stratospheric H_2O variability in the PI simulation between 100 and 30 hPa. In contrast, the 0.1% PAL simulation exhibits a much weaker annual contribution relative to total variance at these pressure levels, consistent with the absence of a tape-recorder signal. Therefore, the seasonal mechanism which transports more water vapour into the stratosphere during warmer periods in the TTL is no longer effective in the 0.1% PAL case.

3.3 Total hydrogen mixing ratio

After H_2O passes through the cold trap, the first bottleneck for the total hydrogen mixing ratio of temperate Earth-like atmospheres has been passed. We now assess the quantitative effect of this bottleneck, and the relative contributions of each of the four major hydrogen bearing species in our simulations.

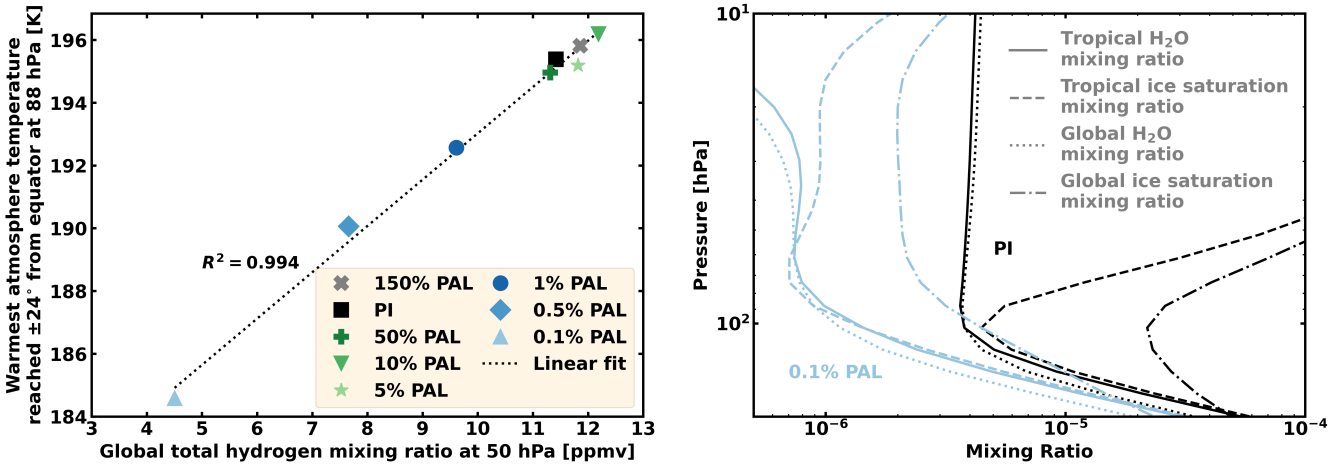

Figure 6. Left: The globally averaged total hydrogen mixing ratio ($f_{\mathrm{T}}(\mathrm{H})$) at 50 hPa is plotted against the warmest temperature reached within $\pm 24^{\circ}$ (tropical latitudes) from the equator at 88 hPa for each simulation. Linear regression gives a coefficient of determination (R^2) of 0.994, which is showed by the dotted black line. The different O_2 mixing ratios are shown by various markers: 150% PAL (grey cross), PI (black square), 50% PAL (dark green plus), 10% PAL (green downward triangle), 5% PAL (light green star), 1% PAL (dark blue circle), 0.5% PAL (blue diamond), and 0.1% PAL (light blue upward triangle). **Right**: The H_2O mixing ratio is plotted against pressure for the PI (black) and 0.1% PAL (light blue) simulations, in terms of its tropical (unbroken line) and global (dotted line) average. Also shown is the ice saturation mixing ratio which depends on temperature and pressure and is shown for the tropical (dashed) and global (dash-dotted) average. The tropical average is for latitudes $\pm 24^{\circ}$ from the equator.

Fig. 6 displays the warmest atmospheric temperature reached in each simulation at a pressure of 88 hPa (≈ 18 km for Earth's atmosphere)[4] in the tropics (within $\pm 24^{\circ}$ from the equator) against the globally averaged $f_{\mathrm{T}}(\mathrm{H})$ at the same pressure level. There is a strong positive correlation with a coefficient of determination of $R^2 = 0.994$ between these two variables. This freeze-drying relationship arises because the warmest temperatures in the tropical atmosphere effectively control the maximum amount of water vapor that can be transported upward through to the stratosphere. As a result, there is a weaker correlation present when comparing $f_{\mathrm{T}}(\mathrm{H})$ with the global mean temperature at the same pressure level, and worse correlation still when comparing to the warmest temperature found anywhere at 88 hPa.

More importantly, Fig. 6 also demonstrates how it is the ice saturation vapor pressure (Murphy and Koop, 2005) in the tropical atmosphere that acts to limit the transport of H_2O upwards. The tropical ice saturation mixing ratio curve is within a factor of 1.18 and 1.01 when compared to the globally averaged H_2O mixing ratio at 100 hPa (≈ 16 km in altitude) for the PI and 0.1% PAL atmospheres, respectively. When comparing the global ice saturation mixing ratio curve, the discrepancy is a factor of 5.8 and 3.9 times, respectively. This means that 1D models that are based on globally averaged temperatures may

[4] 88 hPa is the pressure level in our simulations closest to the winter climatic tropopause of 86-88 hPa, although note that the summer climatic tropopause is closer to 100 hPa (Kim and Son, 2012; Pilch Kedzierski et al., 2016)

overestimate the stratospheric H_2O abundance for Earth-like oxygenated simulations by up to a factor of 6 (accounting for all simulations here, the discrepancy range is 3.8 – 6.0).

Fig. 6 suggests that the warmest TTL temperatures are the controlling factor in each atmospheric scenario, instead of the atmospheric composition. Yet because composition (i.e., the O_2 mixing ratio) is the variable that is altered in each scenario, the atmospheric composition is the controlling factor for the TTL temperatures. Hence, the oxygenation state of the atmosphere is indirectly controlling the upward flow of hydrogen atoms and affecting the diffusion-limited hydrogen escape rate, and this is what we refer to as the 'oxygen valve'.

Fig. 7 presents the globally averaged $f_{\mathrm{T}}(\mathrm{H})$ vertical profile throughout the atmosphere, which is calculated from Eq. 2 for all the simulations. The mixing ratio of total hydrogen in the stratosphere (at 1 hPa) is $f_{\mathrm{T}}(\mathrm{H}) = 11.7$ ppmv in the PI simulation. Turbulent mixing causes $f_{\mathrm{T}}(\mathrm{H})$ to remain roughly constant between the lower stratosphere and homopause. For the 10% PAL, 1% PAL, and 0.1% PAL simulations, the stratospheric $f_{\mathrm{T}}(\mathrm{H})$ values at 1 hPa are approximately 12.4, 6.9, 3.0 ppmv, respectively.

Fig. 7 also shows the total hydrogen contribution from the four species that carry the majority of hydrogen atoms (H, H_2, H_2O, and CH_4). These panels show that for the PI simulation (black lines), H_2O is the primary carrier of hydrogen atoms in the lower atmosphere. Above the cold trap in the TTL, the H_2O mixing ratio increases until it reaches a maximum mesospheric value (≈ 5 ppmv) due to CH_4 reacting with OH. At a pressure of approximately 0.01 hPa, H_2 then becomes dominant. Photolysis of H_2O, CH_4, and H_2, as well as diffusive separation, cause atomic H to become the primary carrier at pressures less than 10^{-4} hPa.

Decreasing levels of O_2 act to shift the pressures at which particular species are the principal hydrogen carrier. H_2 begins to increase in abundance at lower altitudes as the atmospheric O_2 concentration is decreased. For instance, with 1000 times less O_2 (0.1% PAL case, light blue lines), H_2 is dominant at pressures less than 10 hPa, due to both H_2O condensation and photolysis at the higher pressure levels. Again, resulting from diffusive separation, H always dominates towards the top of the model in the lower thermosphere. CH_4 is increasingly lost in the troposphere due to enhanced H_2O photolysis and OH production, acting to reduce CH_4 lifetimes (see the following papers for a more in depth discussion on CH_4 lifetimes: Cooke et al., 2022; Ji et al., 2023; Ji et al., 2024). This loss adds to tropospheric H_2O which is ultimately halted by the cold trap. If the CH_4 mixing ratio at the TTL is greater than half that of H_2O, then CH_4 is the primary contributor to hydrogen escape. However, CH_4 is never the main H carrier in the scenarios we present. As we will discuss later, it is unclear whether this would have been the case for some portions of the Proterozoic.

3.4 Diffusion-limited escape

Now we have assessed $f_{\mathrm{T}}(\mathrm{H})$ throughout the atmosphere we can predict how the rate of diffusion-limited hydrogen escape varies between the different simulated atmospheres with WACCM6. We present the predicted escape rates for each simulation in Table 1.

The $f_{\mathrm{T}}(\mathrm{H})$ profile shows that for the cases with $\leq 1\%$ PAL of O_2, the rate of hydrogen escape is lower than that found in the PI case ($\Phi_{\mathrm{esc,PI}}$). The rates for the 0.1% PAL, 0.5% PAL, and 1% PAL simulations are: $0.26\ \Phi_{\mathrm{esc,PI}}$, $0.57\ \Phi_{\mathrm{esc,PI}}$, and $0.68\ \Phi_{\mathrm{esc,PI}}$,

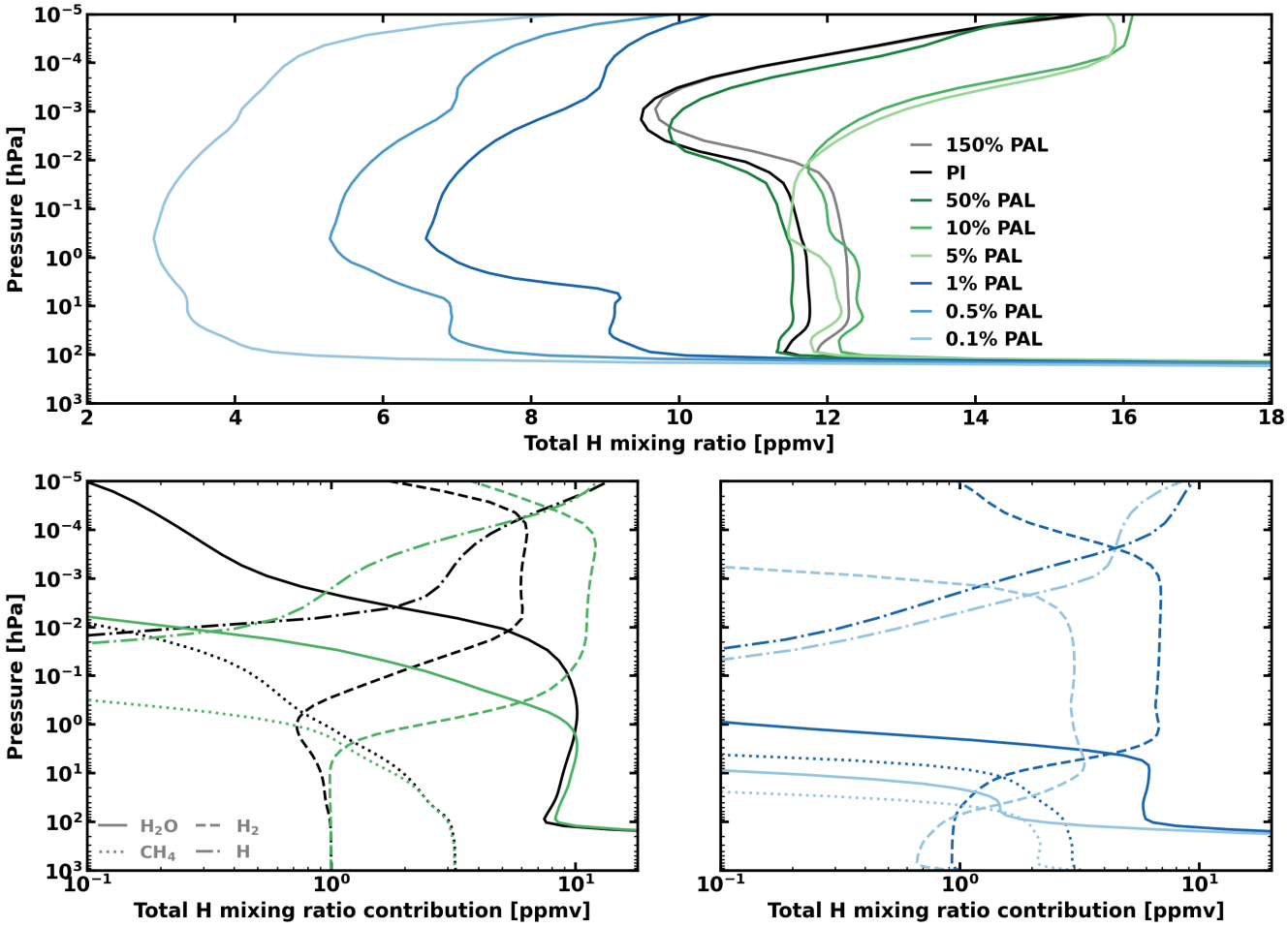

Figure 7. Top: $f_T(H)$, the total hydrogen mixing ratio is given in parts per million by volume (ppmv) and is shown against pressure for the 150% PAL (grey), PI (black), 50% PAL (dark green), 10% PAL (green), 5% PAL (light green), 1% PAL (dark blue), 0.5% PAL (blue), and 0.1% PAL (light blue) simulations. $f_T(H)$ is calculated using Eq. (2). Hence, the mixing ratio contribution from H, H_2O, H_2, and CH_4 is multiplied by a factor of 1, 2, 2, and 4, respectively. **Bottom left**: The total hydrogen mixing ratio contribution from H (dash dotted), H_2 (dashed), H_2O (unbroken), and CH_4 (dotted) is shown for the PI and 10% PAL simulations and **bottom right**: the 1% PAL and 0.1% PAL simulations.

respectively. We also predict that the escape rate could have been slightly higher when O_2 levels were both greater (e.g. 150% PAL) and lesser (e.g. 5 – 10% PAL) than the present day value, with the maximum predicted hydrogen escape rate in the 10% PAL simulation at 1.20 $\Phi_{esc,PI}$. This shows that the TTL heating and predicted escape rate has a non-linear behavior with O_2 concentration. Following the Great Oxidation Event, Earth's O_2 levels are thought to have fluctuated between 0.1% PAL and 150% PAL, although the precise timings and magnitude of these fluctuations are debated (Catling and Zahnle, 2020; Steadman et al., 2020; Planavsky et al., 2020; Yierpan et al., 2020; Krause et al., 2022; Mills et al., 2023; Xie et al., 2023; Fakhraee

Table 1. This table shows the eight simulations where the mixing ratio of O_2, given in terms of present atmospheric level (PAL), was varied. The total hydrogen mixing ratio, $f_T(H)$, in ppmv at the homopause, which is taken to be at a pressure of 10^{-3} hPa. The diffusion-limited hydrogen escape rate is given by Φ_{esc} in mol yr^{-1} and compared to the predicted escape rate in the PI simulation ($\Phi_{esc,PI}$).

Simulation	O_2 [PAL]	Homopause $f_T(H)$ [ppmv]	Φ_{esc} [mol yr^{-1}]	$\Phi_{esc}/\Phi_{esc,PI}$
150% PAL	1.500	9.68	7.71×10^{10}	1.02
PI	1.000	9.52	7.54×10^{10}	1.00
50% PAL	0.500	10.05	7.79×10^{10}	1.03
10% PAL	0.100	12.74	9.04×10^{10}	1.20
5% PAL	0.050	13.07	8.95×10^{10}	1.19
1% PAL	0.010	8.45	5.11×10^{10}	0.68
0.5% PAL	0.005	6.92	3.89×10^{10}	0.57
0.1% PAL	0.001	4.09	1.94×10^{10}	0.26

and Planavsky, 2024; Stockey et al., 2024), with these fluctuations being due to various physical factors, such as carbonate amassing in the crust (Alcott et al., 2024), and large igneous province volcanism combined with weathering (Luo et al., 2024).

4 Discussion

When the Great Oxidation Event occurred approximately 2.4 billion years ago, O_2 increased by several orders of magnitude in the atmosphere in a time frame of approximately 200 Myr (Gumsley et al., 2017). For the first time, these higher levels of O_2 resulted in the generation of a significant O_3 layer which may have created a stratospheric thermal inversion (Kasting et al., 1985; Segura et al., 2003; Cooke et al., 2022). The O_3 layer provided an additional shield for Earth's surface from ultraviolet radiation. However, the exact thickness of the O_3 layer over geological time is difficult to determine. Many uncertainties exist upon the atmospheric pressure and composition throughout the Proterozoic (Lyons et al., 2014; Steadman et al., 2020; Catling and Zahnle, 2020), as well as there being differences in model predictions under similar assumptions (Way et al., 2017; Cooke et al., 2022; Yassin Jaziri et al., 2022; Ji et al., 2023, 2024). With an oxygenated biosphere, the conditions were set for the evolution of oxygen-dependent animals (Cole et al., 2020) and the eventual colonization of land (Dunn, 2013). Additionally, the GOE may have coincided with the end of relatively high levels of hydrogen escape (Zahnle et al., 2013, 2019). Whether other terrestrial worlds go through a similar path of geological and atmospheric evolution is unknown, although it has been modelled under different conditions and assumptions (Gebauer et al., 2018; Olson et al., 2018a; Ozaki and Reinhard, 2021; Krissansen-Totton et al., 2021; Krissansen-Totton and Fortney, 2022).

Our work represents an initial step towards a quantitative estimate for hydrogen escape since the Proterozoic began 2.4 billion years ago. Overall, our results suggest that hydrogen escape during the Proterozoic could have been between 3.8 times lower and up to 1.2 times greater than the calculated pre-industrial escape rate when accounting for O_2 changes only. The present day loss of hydrogen is insignificant on geological timescales, such that the fluctuations in O_2 from the start of the

Proterozoic to the present day likely did not in itself cause substantial levels of hydrogen escape. In what follows, we discuss how our simulations can be used as a platform for future work towards the goal of reconstructing Earth's past atmospheric hydrogen escape.

4.1 The oxygen-ozone valve

When only changing the atmospheric O_2 (and N_2) mixing ratio, as O_2 increases from 0.1% PAL to 150% PAL, the total atmospheric O_3 column increases (Cooke et al., 2022). Note that increasing quantities of total O_3 does not always lead to an increase in temperatures in the TTL, because the location of the O_3 abundance peak in the atmosphere, and the magnitude of the peak, can move with O_2 mixing ratio. This effect is illustrated by the greater total hydrogen mixing ratio at the homopause in the 10% and 5% PAL cases when compared to the PI case (e.g., see Fig. 1, Fig. 6, and Fig. 7).

Our work shows that O_2 levels during the Proterozoic may have partially controlled the diffusion-limited flux for hydrogen escape. However, this will depend on several other factors, such as the continental distribution and the Earth's obliquity which can affect atmospheric dynamics and seasonal cycles, respectively. The fainter Sun, the albedo of the Earth through time, and various greenhouse gases (including CH_4) which can act to cool the stratosphere but warm the surface (Lin and Emanuel, 2024), will have also impacted TTL temperatures and hydrogen escape rates. For instance, a cooling of the stratosphere can increase the amount of O_3, just like the current increasing atmospheric content of CO_2 is aiding a possible, albeit complex, recovery of the O_3 layer (Rosenfield et al., 2002; Fahey et al., 2018; Ivanciu et al., 2022; Maliniemi et al., 2021).

There exist estimates of many of these aforementioned variables through Earth's history, but each of them come with uncertainties and vary throughout the Proterozoic. Liu et al. (2025) suggest that the O_3 layer could have been kept at low levels due to protracted atmospheric iodine concentrations throughout the Proterozoic. Atmospheric iodine would destroy O_3 through catalytic cycles (WACCM6 does not currently include iodine in its chemical mechanism). The computed WACCM6 O_3 columns are lower than the baseline estimates from Liu et al. (2025), but when Liu et al. (2025) included substantial atmospheric iodine (e.g. $20\times$ modern marine iodine concentrations that was emitted to the atmosphere), then their O_3 columns are lower than the WACCM6 results. If we incorporated iodine, then this could lead to a reduced rate of predicted hydrogen escape at a given O_2 concentration due to diminished O_3 heating.

4.2 Model limitations

Our atmospheric predictions are relevant for both Earth's past and future climate states. However, this statement comes with several caveats. The moist-adiabatic lapse rate (the rate at which the temperature of a parcel of saturated air decreases with altitude as it rises in the atmosphere under adiabatic conditions), strongly depends on temperature. Thus, the total hydrogen mixing ratio in the troposphere of the Earth is determined by the incoming radiation, albedo, and greenhouse effect. For modern Earth, these parameters are relatively well known. We did not attempt to fully account for all climatic changes since the Proterozoic began; instead, as a first step, we focused on the effect on the escape rate by changing O_2 only. The range of O_2 concentrations we accounted for are relevant to the past 2.4 billion years and are not relevant to the Archean eon (4 – 2.4 Gyr ago) when molecular oxygen was much lower than present day and Proterozoic (2.4 – 0.541 Gyr ago) concentrations (Catling

and Zahnle, 2020). We remind the reader that WACCM6 is designed for the modern Earth and the current set of simulations do not account for a faster rotation rate in the past (Zahnle and Walker, 1987; Bartlett and Stevenson, 2016; Laskar et al., 2023) or different continental coverage (Mitchell et al., 2021). Additionally, we note that changes to the orbital parameters, rotation rate, or obliquity, may affect the tape recorder signal.

Since Cooke et al. (2022) was published, Ji et al. (2023) showed that absorption of light by H_2O and CO_2 in the S-R bands, as well as scattering in the S-R bands, are increasingly important at lower atmospheric O_2 mixing ratios. The simulations presented in this work do not include either of these treatments. Some WACCM6 simulations (at 10% PAL, 1% PAL, and 0.1% PAL) with H_2O and CO_2 absorption in the S-R bands were included in Ji et al. (2023), and we also ran some simulations with fixed surface fluxes (e.g. for CH_4). Whilst the absolute mixing ratios do deviate when this absorption is included, the effect of changing O_2 on temperature is stronger. In terms of scattering, Ji et al. (2023) showed that it is most important at $\leq 1\%$ PAL of O_2. Inclusion of scattering will decrease the total O_3 column and likely result in a cooler TTL region. Again, the conclusion that hydrogen escape can be be modified by O_2 concentrations remains unaffected, especially when the prescribed CH_4 mixing ratio sets a minimum on the hydrogen escape rate because it is not cold-trapped. Nevertheless, future simulations where WACCM6 includes both absorption and scattering in the S-R bands will provide more comprehensive atmospheric calculations.

4.3 Future work for Earth

The different climate states that might have existed throughout the Proterozoic and Phanerozoic[5] (0.541 Gyr ago – present day) should be simulated in future work. A hotter troposphere may have existed due to increased amounts of CH_4 or CO_2, or both. In this case, the warmer TTL would have increased hydrogen escape rates by elevating the amount of H_2O reaching the stratosphere. On the other hand, colder temperatures during Earth's glacial periods would cool the tropopause (Graham et al., 2019) and reduce the stratospheric H_2O concentration.

Even with a much colder TTL, CH_4 bypasses the control of the oxygen valve or a colder troposphere because CH_4 does not condense in Earth's atmosphere like H_2O. Thus, the Proterozoic and Phanerozoic hydrogen escape rate could have instead been controlled by the CH_4 abundance rather than the O_2 abundance, assuming that its mixing ratio reaching the TTL was greater than half the mixing ratio of H_2O in the TTL - see Eq. 2. The current problem with evaluating this effect is that estimates for Proterozoic CH_4 concentrations vary by several orders of magnitude (Pavlov et al., 2003; Daines and Lenton, 2016; Zhao et al., 2018; Olson et al., 2018a; Laakso and Schrag, 2019; Catling and Zahnle, 2020; Cadeau et al., 2020) and may be greater or lower than the present day mixing ratio. The thinner simulated O_3 columns found from 3D modeling (Cooke et al., 2022; Yassin Jaziri et al., 2022) and updated 1D calculations (Ji et al., 2024), as well as the inclusion of iodine chemistry (Liu et al., 2025), suggest that more UV radiation would have penetrated deeper into the atmosphere for much of the Proterozoic and potentially resulted in lower CH_4 lifetimes at O_2 concentrations of $\leq 1\%$ PAL. In this situation, greater surface-to-atmosphere fluxes of CH_4 would have been required to sustain current ~ 1 ppmv mixing ratios (such fluxes may not be plausible; Daines

[5]By climate states, here we refer to the variety of factors that would have affected weather, atmospheric circulation systems, and surface temperature. These include glaciations and hotter periods, as well as the various continental land masses, fainter Sun, and greenhouse gas concentrations.

and Lenton, 2016; Olson et al., 2016; Laakso and Schrag, 2019), or the higher estimates that some studies suggest in the region of $\sim 10 - 100$ ppmv (Pavlov et al., 2003; Fiorella and Sheldon, 2017; Zhao et al., 2018; Fakhraee et al., 2019). Closer in time to the present day, CH_4 mixing ratios in the Phanerozoic (0.51 Gyr ago - present day) have been simulated to be between 0.1 – 12 ppmv (Beerling et al., 2009).

Clearly, there is much to still learn about why the different models predict specific atmospheric abundances for molecules such as O_3, which has significant horizontal and vertical variation (Cooke et al., 2022; Yassin Jaziri et al., 2022), and CH_4 (Kasting, 2025). The entire conceivable parameter space has certainly not been fully explored; such endeavors utilising 3D models are welcomed but will likely prove computationally expensive. Attempts to define the CH_4 concentrations in the various geological eons are an important part of the history of hydrogen escape, but for now, the mixing ratio of CH_4 through time remains poorly constrained. Ascertaining its production rate in the Proterozoic will help to establish its concentrations in that eon (Kasting and Ji, 2025).

Eventually, as the Sun's luminosity increases, the Earth will heat up, CO_2 will be sequestered out of the atmosphere through carbonate-silicate weathering, and it is predicted that the Earth will lose all of its water through the moist greenhouse effect approximately 2 Gyr in the future (Kasting et al., 1984; Kasting, 1988; Wolf and Toon, 2014; Ozaki and Reinhard, 2021), although the estimate of the time varies. But before that event occurs, previous studies have predicted that the lack of CO_2 will have a detrimental effect on the biosphere because plants are unable to survive at very low CO_2 concentrations (Lovelock and Whitfield, 1982; Caldeira and Kasting, 1992).

Several calculations of the lifespan of the Earth's biosphere have been attempted (Lovelock and Whitfield, 1982; Caldeira and Kasting, 1992; Franck et al., 2000; Von Bloh et al., 2003; Rushby et al., 2018; Ozaki and Reinhard, 2021; Mello and Friaça, 2023; Graham et al., 2024). For instance, Ozaki and Reinhard (2021) calculated that in 1.08 ± 0.14 billion years ($1\ \sigma$), Earth's atmospheric O_2 will drop to 1% PAL. More recently, Graham et al. (2024) suggested that Earth's biosphere may last for up to 1.6 – 1.86 Gyr. Most of these estimates for biospheric termination are before the Earth is predicted to lose its water and become, by the most basic definition, uninhabitable. As O_2 levels drop following the extinction of photosynthesizing life (Ozaki and Reinhard, 2021), O_3 will decrease, and the upper troposphere and TTL may be colder than under otherwise equivalent conditions, diminishing the amount of hydrogen available in the upper atmosphere which can escape to space and cause irreversible water loss (the future rates of hydrogen escape would likely have a negligible effect on oxidizing the Earth to reverse the loss of O_2 from ceasing photosynthesis). Hence, our results suggest that the ocean loss timescale could be extended. Thus, investigations aiming to assess the lifetime of Earth's future habitability should incorporate a 3D chemistry-climate model that includes comprehensive atmospheric oxygen chemistry and that can adequately represent the 3D movement of air parcels through the TTL. Additionally, it is possible that our WACCM6 simulations could be used as input to a model which has a higher top (lower minimum pressure), such as the WACCM-X model (Liu et al., 2018), or even used as an input into a computational model that explicitly calculates atmospheric escape (e.g., Dong et al., 2018; Schulik and Booth, 2023).

4.4 Future work for exoplanets

Other planets outside of our solar system (exoplanets) may be habitable and evolve life. Whether they can keep liquid water on their surface is crucial for the persistence of habitability as it is currently defined.

The H_2O tropical tape recorder is a stratospheric signal of seasonality, impressing the varying TTL temperatures on the stratospheric H_2O mixing ratio. Prior work showed how a 15% reduction in global O_3 (Xie et al., 2008) could cool the TTL and raise it in height, ultimately weakening the tape recorder signal. Here we find this effect exacerbated further as O_2 and O_3 reduce by orders of magnitude. Transmission spectra of exoplanet atmospheres probe the stratosphere, and whilst beyond the detection limit of today's telescopes, such chemical variability may be detectable with future technology or where exoplanets exhibit higher levels of variation that Earth (e.g., for exoplanets with eccentricity ≥ 0.4 Liu et al., 2023) or different types of stratospheric variability (Cohen et al., 2022). Seasonality of biosignatures and other gases (Olson et al., 2018b), combined with the H_2O tape recorder signal, may aid in determining whether a planet is inhabited. Should there be no tape recorder signal due to a tropopause that does not significantly vary with seasons, then this variability will be more difficult to observe, and H_2O will be harder to constrain due to a dry middle-upper atmosphere.

Simulations with other 3D models such as the LMD-g (Yassin Jaziri et al., 2022) or the Unified Model (Braam et al., 2022), or those at higher resolutions (e.g., LFRic-Atmosphere; Sergeev et al., 2023), may yield different quantitative results due to varying treatments of convection and water vapour microphysics, as well as alternative radiative transfer schemes. The stratospheric thermal inversion in Earth's atmosphere is due to O_3 which provides sufficient atmospheric heating when O_2 is present in quantities $\gtrsim 0.1\%$ PAL (Way et al., 2017; Cooke et al., 2022). But a terrestrial exoplanet may not require O_2 to modulate the thermal structure: other atmospheric compositions can result in thermal inversions and may similarly act to enhance or reduce water loss. For example, Titan has a thermal inversion due to the prescence of hazes which absorb shortwave radiation (Danielson et al., 1973; Catling and Kasting, 2017), and CN on hot super-Earths can also cause a thermal inversion (Zilinskas et al., 2021). Additionally, the heating rates will change depending on the distribution of stellar radiation over wavelengths: O_3 radiative heating significantly affects planets around F and G stars but less so around M and K stars (Godolt et al., 2015; Kozakis et al., 2022; De Luca et al., 2024). O_2 can also build up on exoplanets without the presence of life under specific conditions due to large amounts of CO_2 (Segura et al., 2007) or H_2O photolysis (Wordsworth and Pierrehumbert, 2014).

There are various planetary system parameters which affect the climate state of exoplanets. Crucial to the atmospheric dynamics is the planetary rotation rate and whether it is tidally locked (Forget and Leconte, 2014; Turbet et al., 2016; Boutle et al., 2017; Del Genio et al., 2019b; Braam et al., 2025). The circulation affects the atmospheric temperature structure and how tracers such as H_2O are advected. Other salient factors include the strength and spectral shape of the incoming radiation (Eager-Nash et al., 2020), the continental distribution or lack thereof (Lewis et al., 2018; Zhao et al., 2021; Macdonald et al., 2022), obliquity (Kang, 2019), eccentricity (Liu et al., 2023), flares (Chen et al., 2021; Ridgway et al., 2023), simulation resolution (Sergeev et al., 2020; Lefèvre et al., 2021; Song et al., 2022; Kodama et al., 2022; Yang et al., 2023; Sergeev et al., 2024; Garcia et al., 2024), as well as the planetary Bond albedo and surface composition (Cowan and Agol, 2011; Del Genio

et al., 2019a; Madden and Kaltenegger, 2020). Ocean salinity can also be important in modulating the climate of rocky planets (Olson et al., 2022).

By connecting exoplanet simulations to a model that includes the ionosphere (e.g., WACCM-X), one could attempt to answer interesting questions regarding the upper atmospheres of terrestrial exoplanets. For instance, how do the ionospheres of various exoplanets compare to Earth? Just like flares disturb the atmospheres of terrestrial planets (Segura et al., 2010; Tilley et al., 2019; Chen et al., 2021; Ridgway et al., 2023), do flares (especially for active M dwarf stars) impact their ionospheres differently from those that strike the Earth (Leonovich and Tashchilin, 2009; Schillings et al., 2018; Hayes et al., 2021)? And could those differences manifest in a way which is detectable with future instruments (Mendillo et al., 2018; Mendillo, 2019)?

The maximum difference we found in the diffusion-limited hydrogen escape between alternative oxygenation states when all other initial conditions and boundary conditions are kept constant is a factor of 4.7. Whilst this change is not significant for Earth under the assumptions made in this work, it potentially could be significant when the ocean loss timescale for a habitable terrestrial exoplanet is similar to a time that a planet could theoretically spend in the habitable zone (i.e. a planet with a 10 Gyr ocean loss timescale with a different oxygenation state could instead have an ocean loss timescale of ≈ 2 Gyr).

5 Conclusions

Since the dawn of the Proterozoic (2.4 Gyr ago), several properties of the Earth have changed. The continental configuration has shifted several times, the Sun's luminosity has increased, and the concentration of atmospheric gases such as O_2, CO_2, and CH_4 have fluctuated.

This work used WACCM6 simulations of the Earth to explore the effect that the changing O_2 mixing ratio had on the total hydrogen mixing ratio at the homopause in order to predict the possible diffusion-limited hydrogen escape rate through geological time. A 3D model with chemistry and a global representation of water vapour microphysics is critical to simulating the transport of H_2O into the stratosphere and thus estimating diffusion-limited hydrogen escape when other atmospheric constituents (e.g., CH_4 and H_2, which we held constant at the surface) are not the dominant hydrogen bearing species. In our simulated scenarios we showed that 1D models may predict a stratospheric water vapour discrepancy of between a factor of 3.8 – 6.0 depending on the O_2 mixing ratio when compared to 3D calculations.

We found that the atmospheric O_2 mixing ratio acts as a nonlinear valve on the total hydrogen mixing ratio in the stratosphere. The O_3 mixing ratio (which is affected by the abundance of O_2) around the tropical tropopause layer (TTL) determines the amount of UV heating that warms the TTL and controls the H_2O mixing ratio entering the stratosphere. The obliquity of Earth induces seasonal cycles, which affect phenomena such as the Brewer-Dobson circulation and the tropical tape recorder. We showed that the tropical tape recorder disappeared at 0.1% PAL, which suggests that the present-day seasonal transport of H_2O molecules to the stratosphere may not have taken place at low O_2 mixing ratios.

Between 0.1% PAL and 150% PAL of O_2, the upward diffusion of H_2O is modulated in a non-linear manner, with 5% and 10% PAL having the maximum predicted diffusion-limited escape rate of hydrogen due to O_3 concentrations causing localized heating. The predicted escape rate changes by up to a factor of 4.7 between all of the simulations, meaning that whilst the

oxygen valve affects diffusion-limited hydrogen escape, in the absence of other factors, it would not have resulted in relatively high levels of hydrogen escape and thus water loss since the GOE.

In order to dissect Earth's atmospheric history, future work should investigate multiple other physical, chemical, and biological factors that may affect the hydrogen escape rate whilst also accounting for the oxygen valve we presented.

. WACCM6 is a publicly available code. The specific release used in this paper was CESM2.1.3, which can be downloaded from the following CESM downloads page: https://escomp.github.io/CESM/versions/cesm2.1/html/downloading_cesm. Our code modifications are detailed here in the ExoCESM GitHub https://github.com/exo-cesm/CESM2.1.3/tree/main/O2_Earth_analogues.

. The time-averaged data is currently available in the Dryad data repository at https://doi.org/10.5061/dryad.ncjsxksvn. The data with time-variability will be made available upon acceptance of the manuscript.

. GJC set up and ran the simulations, performed the analysis, wrote the analysis and plotting code, and wrote the manuscript. DRM and CW supervised the project and provided comments on the manuscript. FSM and MB provided comments on the manuscript.

. The authors declare no competing interests

. G.J.C. thanks the Science and Technology Facilities Council for financial support during the PhD when the simulations were conducted (grant number ST/T506230/1). G.J.C. thanks James Rogers and Oli Shorttle for helpful discussions regarding Earth's history and hydrogen escape. F. Sainsbury-Martinez and C. Walsh would like to thank UK Research and Innovation for support under grant number MR/Z00019X/1 Additionally, C. Walsh would like to thank the University of Leeds and the Science and Technology Facilities Council for financial support (ST/X001016/1). M.B. appreciates support from a CSH Postdoctoral Fellowship. This work was undertaken on ARC4, part of the High Performance Computing facilities at the University of Leeds, UK. The CESM project is supported primarily by the U.S. National Science Foundation.

References

Alcott, L. J., Walton, C., Planavsky, N. J., Shorttle, O., and Mills, B. J. W.: Crustal carbonate build-up as a driver for Earth's oxygenation, Nature Geoscience, 17, 458–464, https://doi.org/10.1038/s41561-024-01417-1, 2024.

Anders, E. and Owen, T.: Mars and Earth: Origin and Abundance of Volatiles, Science, 198, 453–465, https://doi.org/10.1126/science.198.4316.453, 1977.

Avice, G., Marty, B., Burgess, R., Hofmann, A., Philippot, P., Zahnle, K., and Zakharov, D.: Evolution of atmospheric xenon and other noble gases inferred from Archean to Paleoproterozoic rocks, GeoCoA, 232, 82–100, https://doi.org/10.1016/j.gca.2018.04.018, 2018.

Bahcall, J. N., Pinsonneault, M., and Basu, S.: Solar models: Current epoch and time dependences, neutrinos, and helioseismological properties, The Astrophysical Journal, 555, 990, 2001.

Banks, P. and Kockarts, G.: Aeronomy, volume 2, 263 pp, 1973.

Bartlett, B. C. and Stevenson, D. J.: Analysis of a Precambrian resonance-stabilized day length, Geophys. Res. Lett., 43, 5716–5724, https://doi.org/10.1002/2016GL068912, 2016.

Beerling, D., Berner, R. A., Mackenzie, F. T., Harfoot, M. B., and Pyle, J. A.: Methane and the CH 4 related greenhouse effect over the past 400 million years, American Journal of Science, 309, 97–113, 2009.

Boutle, I. A., Mayne, N. J., Drummond, B., Manners, J., Goyal, J., Hugo Lambert, F., Acreman, D. M., and Earnshaw, P. D.: Exploring the climate of Proxima B with the Met Office Unified Model, A&A, 601, A120, https://doi.org/10.1051/0004-6361/201630020, 2017.

Braam, M., Palmer, P. I., Decin, L., Ridgway, R. J., Zamyatina, M., Mayne, N. J., Sergeev, D. E., and Abraham, N. L.: Lightning-induced chemistry on tidally-locked Earth-like exoplanets, MNRAS, 517, 2383–2402, https://doi.org/10.1093/mnras/stac2722, 2022.

Braam, M., Palmer, P. I., Decin, L., Mayne, N. J., Manners, J., and Rugheimer, S.: Earth-like Exoplanets in Spin–Orbit Resonances: Climate Dynamics, 3D Atmospheric Chemistry, and Observational Signatures, PSJ, 6, 5, https://doi.org/10.3847/PSJ/ad9565, 2025.

Brasseur, G. P. and Solomon, S.: Aeronomy of the Middle Atmosphere: Chemistry and Physics of the Stratosphere and Mesosphere, Springer Dordrecht, 2005.

Brewer, A. W.: Evidence for a world circulation provided by the measurements of helium and water vapour distribution in the stratosphere, Quarterly Journal of the Royal Meteorological Society, 75, 351–363, https://doi.org/10.1002/qj.49707532603, 1949.

Butchart, N.: The Brewer-Dobson circulation, Reviews of Geophysics, 52, 157–184, https://doi.org/10.1002/2013RG000448, 2014.

Cadeau, P., Jézéquel, D., Leboulanger, C., Fouilland, E., Le Floc'h, E., Chaduteau, C., Milesi, V., Guélard, J., Sarazin, G., Katz, A., et al.: Carbon isotope evidence for large methane emissions to the Proterozoic atmosphere, Scientific reports, 10, 18 186, 2020.

Caldeira, K. and Kasting, J. F.: The life span of the biosphere revisited, Nature, 360, 721–723, https://doi.org/10.1038/360721a0, 1992.

Cangi, E. M., Chaffin, M., Gregory, B., Yelle, R. V., Deighan, J., Elliott, R., and Gröller, H.: Venus Water Loss is Dominated by HCO+ Dissociative Recombination, in: AGU Fall Meeting Abstracts, vol. 2024 of *AGU Fall Meeting Abstracts*, pp. SM13E–08, 2024.

Catling, D. C. and Kasting, J. F.: Atmospheric Evolution on Inhabited and Lifeless Worlds, Cambridge University Press, 2017.

Catling, D. C. and Kasting, J. F.: Atmospheric evolution on inhabited and lifeless worlds, Cambridge University Press, 2017.

Catling, D. C. and Zahnle, K. J.: The Archean atmosphere, Science Advances, 6, eaax1420, https://doi.org/10.1126/sciadv.aax1420, 2020.

Catling, D. C., Zahnle, K. J., and McKay, C. P.: Biogenic Methane, Hydrogen Escape, and the Irreversible Oxidation of Early Earth, Science, 293, 839–843, https://doi.org/10.1126/science.1061976, 2001.

Charette, M. A. and Smith, W. H.: The volume of Earth's ocean, Oceanography, 23, 112–114, 2010.

Charnay, B., Wolf, E. T., Marty, B., and Forget, F.: Is the Faint Young Sun Problem for Earth Solved?, SSRv, 216, 90, https://doi.org/10.1007/s11214-020-00711-9, 2020.

Chen, H., Zhan, Z., Youngblood, A., Wolf, E. T., Feinstein, A. D., and Horton, D. E.: Persistence of flare-driven atmospheric chemistry on rocky habitable zone worlds, Nature Astronomy, 5, 298–310, https://doi.org/10.1038/s41550-020-01264-1, 2021.

Claire, M. W., Catling, D. C., and Zahnle, K. J.: Biogeochemical modelling of the rise in atmospheric oxygen, Geobiology, 4, 239–269, 2006.

Cohen, M., Bollasina, M. A., Palmer, P. I., Sergeev, D. E., Boutle, I. A., Mayne, N. J., and Manners, J.: Longitudinally Asymmetric Stratospheric Oscillation on a Tidally Locked Exoplanet, ApJ, 930, 152, https://doi.org/10.3847/1538-4357/ac625d, 2022.

Cole, D. B., Mills, D. B., Erwin, D. H., Sperling, E. A., Porter, S. M., Reinhard, C. T., and Planavsky, N. J.: On the co-evolution of surface oxygen levels and animals, Geobiology, 18, 260–281, https://doi.org/10.1111/gbi.12382, 2020.

Constantinou, T., Shorttle, O., and Rimmer, P. B.: A dry Venusian interior constrained by atmospheric chemistry, Nature Astronomy, https://doi.org/10.1038/s41550-024-02414-5, 2024.

Cooke, G. J., Marsh, D. R., Walsh, C., Black, B., and Lamarque, J. F.: A revised lower estimate of ozone columns during Earth's oxygenated history, Royal Society Open Science, 9, 211165, https://doi.org/10.1098/rsos.211165, 2022.

Cowan, N. B. and Agol, E.: The Statistics of Albedo and Heat Recirculation on Hot Exoplanets, ApJ, 729, 54, https://doi.org/10.1088/0004-637X/729/1/54, 2011.

Daines, S. J. and Lenton, T. M.: The effect of widespread early aerobic marine ecosystems on methane cycling and the Great Oxidation, Earth and Planetary Science Letters, 434, 42–51, https://doi.org/10.1016/j.epsl.2015.11.021, 2016.

Daines, S. J. and Lenton, T. M.: The effect of widespread early aerobic marine ecosystems on methane cycling and the Great Oxidation, Earth and Planetary Science Letters, 434, 42–51, 2016.

Danielsen, E. F.: A dehydration mechanism for the stratosphere, Geophys. Res. Lett., 9, 605–608, https://doi.org/10.1029/GL009i006p00605, 1982.

Danielson, R. E., Caldwell, J. J., and Larach, D. R.: An Inversion in the Atmosphere of Titan, Icarus, 20, 437–443, https://doi.org/10.1016/0019-1035(73)90016-X, 1973.

Dauphas, N., Robert, F., and Marty, B.: The Late Asteroidal and Cometary Bombardment of Earth as Recorded in Water Deuterium to Protium Ratio, Icarus, 148, 508–512, https://doi.org/10.1006/icar.2000.6489, 2000.

De Luca, P., Braam, M., Komacek, T. D., and Hochman, A.: The impact of ozone on Earth-like exoplanet climate dynamics: the case of Proxima Centauri b, MNRAS, 531, 1471–1482, https://doi.org/10.1093/mnras/stae1199, 2024.

Deitrick, R. and Goldblatt, C.: Effects of ozone levels on climate through Earth history, Climate of the Past, 19, 1201–1218, https://doi.org/10.5194/cp-19-1201-2023, 2023.

Del Genio, A. D., Kiang, N. Y., Way, M. J., Amundsen, D. S., Sohl, L. E., Fujii, Y., Chandler, M., Aleinov, I., Colose, C. M., Guzewich, S. D., and Kelley, M.: Albedos, Equilibrium Temperatures, and Surface Temperatures of Habitable Planets, ApJ, 884, 75, https://doi.org/10.3847/1538-4357/ab3be8, 2019a.

Del Genio, A. D., Way, M. J., Amundsen, D. S., Aleinov, I., Kelley, M., Kiang, N. Y., and Clune, T. L.: Habitable Climate Scenarios for Proxima Centauri b with a Dynamic Ocean, Astrobiology, 19, 99–125, https://doi.org/10.1089/ast.2017.1760, 2019b.

Dessler, A. E.: A reexamination of the "stratospheric fountain" hypothesis, Geophys. Res. Lett., 25, 4165–4168, https://doi.org/10.1029/1998GL900120, 1998.

di Achille, G. and Hynek, B. M.: Ancient ocean on Mars supported by global distribution of deltas and valleys, Nature Geoscience, 3, 459–463, https://doi.org/10.1038/ngeo891, 2010.

Dobson, G. M. B. and Harrison, D. N.: Measurements of the Amount of Ozone in the Earth's Atmosphere and Its Relation to Other Geophysical Conditions, Proceedings of the Royal Society of London Series A, 110, 660–693, https://doi.org/10.1098/rspa.1926.0040, 1926.

Dong, C., Jin, M., Lingam, M., Airapetian, V. S., Ma, Y., and van der Holst, B.: Atmospheric escape from the TRAPPIST-1 planets and implications for habitability, Proceedings of the National Academy of Science, 115, 260–265, https://doi.org/10.1073/pnas.1708010115, 2018.

Dong, J., Fischer, R. A., Stixrude, L. P., and Lithgow-Bertelloni, C. R.: Constraining the Volume of Earth's Early Oceans With a Temperature Dependent Mantle Water Storage Capacity Model, AGU Advances, 2, e2020AV000323, https://doi.org/10.1029/2020AV000323, 2021.

Dong, W. H., Lin, Y. L., Zhang, M. H., and Huang, X. M.: Footprint of Tropical Mesoscale Convective System Variability on Stratospheric Water Vapor, Geophys. Res. Lett., 47, e86320, https://doi.org/10.1029/2019GL086320, 2020.

Dunn, C. W.: Evolution: out of the ocean, Current Biology, 23, R241–R243, 2013.

Eager-Nash, J. K., Reichelt, D. J., Mayne, N. J., Hugo Lambert, F., Sergeev, D. E., Ridgway, R. J., Manners, J., Boutle, I. A., Lenton, T. M., and Kohary, K.: Implications of different stellar spectra for the climate of tidally locked Earth-like exoplanets, A&A, 639, A99, https://doi.org/10.1051/0004-6361/202038089, 2020.

Emmons, L. K., Schwantes, R. H., Orlando, J. J., Tyndall, G., Kinnison, D., Lamarque, J.-F., Marsh, D., Mills, M. J., Tilmes, S., Bardeen, C., Buchholz, R. R., Conley, A., Gettelman, A., Garcia, R., Simpson, I., Blake, D. R., Meinardi, S., and Pétron, G.: The Chemistry Mechanism in the Community Earth System Model Version 2 (CESM2), Journal of Advances in Modeling Earth Systems, 12, e2019MS001882, https://doi.org/10.1029/2019MS001882, 2020.

Fahey, D., Newman, P. A., Pyle, J. A., Safari, B., Chipperfield, M. P., Karoly, D., Kinnison, D. E., Ko, M., Santee, M., and Doherty, S. J.: Scientific assessment of ozone depletion: 2018, global ozone research and monitoring project-report no. 58, 2018.

Fakhraee, M. and Planavsky, N.: Insights from a dynamical system approach into the history of atmospheric oxygenation, Nature Communications, 15, 6794, https://doi.org/10.1038/s41467-024-51042-0, 2024.

Fakhraee, M., Hancisse, O., Canfield, D. E., Crowe, S. A., and Katsev, S.: Proterozoic seawater sulfate scarcity and the evolution of ocean–atmosphere chemistry, Nature Geoscience, 12, 375–380, 2019.

Farquhar, J., Bao, H., and Thiemens, M.: Atmospheric Influence of Earth's Earliest Sulfur Cycle, Science, 289, 756–759, https://doi.org/10.1126/science.289.5480.756, 2000.

Feulner, G.: The faint young Sun problem, Reviews of Geophysics, 50, RG2006, https://doi.org/10.1029/2011RG000375, 2012.

Fiorella, R. P. and Sheldon, N. D.: Equable end Mesoproterozoic climate in the absence of high CO2, Geology, 45, 231–234, https://doi.org/10.1130/G38682.1, 2017.

Forget, F. and Leconte, J.: Possible climates on terrestrial exoplanets, Philosophical Transactions of the Royal Society of London Series A, 372, 20130 084–20130 084, https://doi.org/10.1098/rsta.2013.0084, 2014.

Forster, P. M., Bodeker, G., Schofield, R., Solomon, S., and Thompson, D.: Effects of ozone cooling in the tropical lower stratosphere and upper troposphere, Geophys. Res. Lett., 34, L23813, https://doi.org/10.1029/2007GL031994, 2007.

Franck, S., Block, A., Von Bloh, W., Bounama, C., Schellnhuber, H. J., and Svirezhev, Y.: Reduction of biosphere life span as a consequence of geodynamics, Tellus Series B Chemical and Physical Meteorology B, 52, 94–107, https://doi.org/10.3402/tellusb.v52i1.16085, 2000.

Fueglistaler, S., Dessler, A. E., Dunkerton, T. J., Folkins, I., Fu, Q., and Mote, P. W.: Tropical tropopause layer, Reviews of Geophysics, 47, RG1004, https://doi.org/10.1029/2008RG000267, 2009.

Garcia, V., Smith, C. M., Chavas, D. R., and Komacek, T. D.: Tropical Cyclones on Tidally Locked Rocky Planets: Dependence on Rotation Period, ApJ, 965, 5, https://doi.org/10.3847/1538-4357/ad2ea5, 2024.

Gardner, J. V., Armstrong, A. A., Calder, B. R., and Beaudoin, J.: So, how deep is the Mariana Trench?, Marine Geodesy, 37, 1–13, 2014.

Garfinkel, C. I., Waugh, D. W., Oman, L. D., Wang, L., and Hurwitz, M. M.: Temperature trends in the tropical upper troposphere and lower stratosphere: Connections with sea surface temperatures and implications for water vapor and ozone, Journal of Geophysical Research (Atmospheres), 118, 9658–9672, https://doi.org/10.1002/jgrd.50772, 2013.

Gebauer, S., Grenfell, J. L., Lehmann, R., and Rauer, H.: Evolution of Earth-like Planetary Atmospheres around M Dwarf Stars: Assessing the Atmospheres and Biospheres with a Coupled Atmosphere Biogeochemical Model, Astrobiology, 18, 856–872, https://doi.org/10.1089/ast.2017.1723, 2018.

Genda, H. and Ikoma, M.: Origin of the ocean on the Earth: Early evolution of water D/H in a hydrogen-rich atmosphere, Icarus, 194, 42–52, https://doi.org/10.1016/j.icarus.2007.09.007, 2008.

Gettelman, A., Mills, M. J., Kinnison, D. E., Garcia, R. R., Smith, A. K., Marsh, D. R., Tilmes, S., Vitt, F., Bardeen, C. G., McInerny, J., Liu, H. L., Solomon, S. C., Polvani, L. M., Emmons, L. K., Lamarque, J. F., Richter, J. H., Glanville, A. S., Bacmeister, J. T., Phillips, A. S., Neale, R. B., Simpson, I. R., DuVivier, A. K., Hodzic, A., and Randel, W. J.: The Whole Atmosphere Community Climate Model Version 6 (WACCM6), Journal of Geophysical Research (Atmospheres), 124, 12,380–12,403, https://doi.org/10.1029/2019JD030943, 2019.

Glanville, A. A. and Birner, T.: Role of vertical and horizontal mixing in the tape recorder signal near the tropical tropopause, Atmospheric Chemistry & Physics, 17, 4337–4353, https://doi.org/10.5194/acp-17-4337-2017, 2017.

Godolt, M., Grenfell, J. L., Hamann-Reinus, A., Kitzmann, D., Kunze, M., Langematz, U., von Paris, P., Patzer, A. B. C., Rauer, H., and Stracke, B.: 3D climate modeling of Earth-like extrasolar planets orbiting different types of host stars, Planet. Space Sci., 111, 62–76, https://doi.org/10.1016/j.pss.2015.03.010, 2015.

Goldblatt, C., McDonald, V. L., and McCusker, K. E.: Earth's long-term climate stabilized by clouds, Nature Geoscience, 14, 143–150, https://doi.org/10.1038/s41561-021-00691-7, 2021.

Goldblatt, C., McDonald, V. L., and McCusker, K. E.: Earth's long-term climate stabilized by clouds, Nature Geoscience, 14, 143–150, 2021.

Graham, R. J., Shaw, T. A., and Abbot, D. S.: The Snowball Stratosphere, Journal of Geophysical Research (Atmospheres), 124, 11,819–11,836, https://doi.org/10.1029/2019JD031361, 2019.

Graham, R. J., Halevy, I., and Abbot, D.: Substantial Extension of the Lifetime of the Terrestrial Biosphere, PSJ, 5, 255, https://doi.org/10.3847/PSJ/ad7856, 2024.

Gronoff, G., Arras, P., Baraka, S., Bell, J. M., Cessateur, G., Cohen, O., Curry, S. M., Drake, J. J., Elrod, M., Erwin, J., Garcia-Sage, K., Garraffo, C., Glocer, A., Heavens, N. G., Lovato, K., Maggiolo, R., Parkinson, C. D., Simon Wedlund, C., Weimer, D. R., and Moore, W. B.: Atmospheric Escape Processes and Planetary Atmospheric Evolution, Journal of Geophysical Research (Space Physics), 125, e27639, https://doi.org/10.1029/2019JA02763910.1002/essoar.10502458.1, 2020.

Gu, H., Cui, J., Wu, X., Huang, X., Wu, S., Li, W., Zhao, J., Lu, H., and Li, L.: Hydrogen Loss on Venus Driven by Photochemistry, ApJL, 988, L31, https://doi.org/10.3847/2041-8213/adec90, 2025.

Gumsley, A. P., Chamberlain, K. R., Bleeker, W., Söderlund, U., de Kock, M. O., Larsson, E. R., and Bekker, A.: Timing and tempo of the Great Oxidation Event, Proceedings of the National Academy of Science, 114, 1811–1816, https://doi.org/10.1073/pnas.1608824114, 2017.

Hallis, L. J., Huss, G. R., Nagashima, K., Taylor, G. J., Halldórsson, S. A., Hilton, D. R., Mottl, M. J., and Meech, K. J.: Evidence for primordial water in Earth's deep mantle, Science, 350, 795–797, https://doi.org/10.1126/science.aac4834, 2015.

Hayes, L. A., O'Hara, O. S. D., Murray, S. A., and Gallagher, P. T.: Solar Flare Effects on the Earth's Lower Ionosphere, SoPh, 296, 157, https://doi.org/10.1007/s11207-021-01898-y, 2021.

Hodgskiss, M. S. W., Crockford, P. W., Peng, Y., Wing, B. A., and Horner, T. J.: A productivity collapse to end Earth's Great Oxidation, Proceedings of the National Academy of Science, 116, 17 207–17 212, https://doi.org/10.1073/pnas.1900325116, 2019.

Holland, H. D.: Volcanic gases, black smokers, and the great oxidation event, GeoCoA, 66, 3811–3826, https://doi.org/10.1016/S0016-7037(02)00950-X, 2002.

Hunten, D. M.: The Escape of Light Gases from Planetary Atmospheres., Journal of the Atmospheric Sciences, 30, 1481–1494, https://doi.org/10.1175/1520-0469(1973)030<1481:TEOLGF>2.0.CO;2, 1973.

Hunten, D. M. and Donahue, T. M.: Hydrogen Loss from the Terrestrial Planets, Annual Review of Earth and Planetary Sciences, 4, 265, https://doi.org/10.1146/annurev.ea.04.050176.001405, 1976.

Ingersoll, A. P.: The Runaway Greenhouse: A History of Water on Venus., Journal of the Atmospheric Sciences, 26, 1191–1198, https://doi.org/10.1175/1520-0469(1969)026<1191:TRGAHO>2.0.CO;2, 1969.

Ivanciu, I., Matthes, K., Biastoch, A., Wahl, S., and Harlaß, J.: Twenty-first-century Southern Hemisphere impacts of ozone recovery and climate change from the stratosphere to the ocean, Weather and Climate Dynamics, 3, 139–171, https://doi.org/10.5194/wcd-3-139-2022, 2022.

Izidoro, A., de Souza Torres, K., Winter, O. C., and Haghighipour, N.: A Compound Model for the Origin of Earth's Water, ApJ, 767, 54, https://doi.org/10.1088/0004-637X/767/1/54, 2013.

Ji, A., Kasting, J., Cooke, G., Marsh, D., and Tsigaridis, K.: Comparison between ozone column depths and methane lifetimes computed by one-and three-dimensional models at different atmospheric O2 levels, Royal Society Open Science, 10, 230 056, 2023.

Ji, A., Kasting, J. F., Cooke, G. J., Marsh, D. R., and Tsigaridis, K.: Comparison between ozone column depths and methane lifetimes computed by one- and three-dimensional models at different atmospheric O_2 levels, Royal Society Open Science, 10, 230056, https://doi.org/10.1098/rsos.230056, 2023.

Ji, A., Tomazzeli, O. G., Palancar, G. G., Chaverot, G., Barker, M., Fernández, R. P., Minschwaner, K., and Kasting, J. F.: A Correlated-K Parameterization for O_2 Photolysis in the Schumann-Runge Bands, Journal of Geophysical Research (Atmospheres), 129, e2023JD040610, https://doi.org/10.1029/2023JD040610, 2024.

Johnson, R. E.: Thermally Driven Atmospheric Escape, ApJ, 716, 1573–1578, https://doi.org/10.1088/0004-637X/716/2/1573, 2010.

Kadoya, S. and Catling, D. C.: Constraints on hydrogen levels in the Archean atmosphere based on detrital magnetite, GeoCoA, 262, 207–219, https://doi.org/10.1016/j.gca.2019.07.041, 2019.

Kaltenegger, L., Lin, Z., and Rugheimer, S.: Finding Signs of Life on Transiting Earthlike Planets: High-resolution Transmission Spectra of Earth through Time around FGKM Host Stars, ApJ, 904, 10, https://doi.org/10.3847/1538-4357/abb9b2, 2020.

Kane, S. R., Arney, G., Crisp, D., Domagal-Goldman, S., Glaze, L. S., Goldblatt, C., Grinspoon, D., Head, J. W., Lenardic, A., Unterborn, C., Way, M. J., and Zahnle, K. J.: Venus as a Laboratory for Exoplanetary Science, Journal of Geophysical Research (Planets), 124, 2015–2028, https://doi.org/10.1029/2019JE005939, 2019.

Kang, W.: Wetter Stratospheres on High-obliquity Planets, ApJL, 877, L6, https://doi.org/10.3847/2041-8213/ab1f79, 2019.

Kanzaki, Y. and Murakami, T.: Estimates of atmospheric CO2 in the Neoarchean–Paleoproterozoic from paleosols, Geochimica et Cosmochimica Acta, 159, 190–219, 2015.

Kasting, J. F.: Runaway and moist greenhouse atmospheres and the evolution of Earth and Venus, Icarus, 74, 472–494, https://doi.org/10.1016/0019-1035(88)90116-9, 1988.

Kasting, J. F.: THE EVOLUTION OF ATMOSPHERIC COMPOSITION AND CLIMATE: WHY EARTH IS A HABITABLE PLANET, Geochemical Perspectives, 14, 1–2, 2025.

Kasting, J. F. and Catling, D.: Evolution of a Habitable Planet, ARA&A, 41, 429–463, https://doi.org/10.1146/annurev.astro.41.071601.170049, 2003.

Kasting, J. F. and Ji, A.: Atmospheric oxygen and methane on the early Earth, Philosophical Transactions B, 380, 20240 093, 2025.

Kasting, J. F., Pollack, J. B., and Ackerman, T. P.: Response of Earth's atmosphere to increases in solar flux and implications for loss of water from Venus, Icarus, 57, 335–355, https://doi.org/10.1016/0019-1035(84)90122-2, 1984.

Kasting, J. F., Holland, H. D., and Pinto, J. P.: Oxidant abundances in rainwater and the evolution of atmospheric oxygen, Journal of Geophysical Research: Atmospheres, 90, 10 497–10 510, 1985.

Kasting, J. F., Pavlov, A. A., and Siefert, J. L.: A Coupled Ecosystem-Climate Model for Predicting the Methane Concentration in the Archean Atmosphere, Origins of Life and Evolution of the Biosphere, 31, 271–285, https://doi.org/10.1023/A:1010600401718, 2001.

Kasting, J. F., Chen, H., and Kopparapu, R. K.: Stratospheric Temperatures and Water Loss from Moist Greenhouse Atmospheres of Earth-like Planets, ApJL, 813, L3, https://doi.org/10.1088/2041-8205/813/1/L3, 2015.

Kharecha, P., Kasting, J., and Siefert, J.: A coupled atmosphere–ecosystem model of the early Archean Earth, Geobiology, 3, 53–76, 2005.

Kim, J. and Son, S.-W.: Tropical cold-point tropopause: Climatology, seasonal cycle, and intraseasonal variability derived from COSMIC GPS radio occultation measurements, Journal of Climate, 25, 5343–5360, 2012.

Kodama, T., Takasuka, D., Sherriff-Tadano, S., Kuroda, T., Miyakawa, T., Abe-Ouchi, A., and Satoh, M.: Climate of High-obliquity Exoterrestrial Planets with a Three-dimensional Cloud System Resolving Climate Model, ApJ, 940, 87, https://doi.org/10.3847/1538-4357/ac98ae, 2022.

Korenaga, J., Planavsky, N. J., and Evans, D. A. D.: Global water cycle and the coevolution of the Earth's interior and surface environment, Philosophical Transactions of the Royal Society of London Series A, 375, 20150393, https://doi.org/10.1098/rsta.2015.0393, 2017.

Kozakis, T., Mendonça, J. M., and Buchhave, L. A.: Is ozone a reliable proxy for molecular oxygen?. I. The O_2-O_3 relationship for Earth-like atmospheres, A&A, 665, A156, https://doi.org/10.1051/0004-6361/202244164, 2022.

Krause, A. J., Mills, B. J., Merdith, A. S., Lenton, T. M., and Poulton, S. W.: Extreme variability in atmospheric oxygen levels in the late Precambrian, Science advances, 8, eabm8191, 2022.

Krissansen-Totton, J. and Fortney, J. J.: Predictions for Observable Atmospheres of Trappist-1 Planets from a Fully Coupled Atmosphere-Interior Evolution Model, ApJ, 933, 115, https://doi.org/10.3847/1538-4357/ac69cb, 2022.

Krissansen-Totton, J., Fortney, J. J., Nimmo, F., and Wogan, N.: Oxygen False Positives on Habitable Zone Planets Around Sun-Like Stars, AGU Advances, 2, e00294, https://doi.org/10.1029/2020AV000294, 2021.

Kulikov, Y. N., Lammer, H., Lichtenegger, H. I. M., Terada, N., Ribas, I., Kolb, C., Langmayr, D., Lundin, R., Guinan, E. F., Barabash, S., and Biernat, H. K.: Atmospheric and water loss from early Venus, Planet. Space Sci., 54, 1425–1444, https://doi.org/10.1016/j.pss.2006.04.021, 2006.

Kurokawa, H., Foriel, J., Laneuville, M., Houser, C., and Usui, T.: Subduction and atmospheric escape of Earth's seawater constrained by hydrogen isotopes, Earth and Planetary Science Letters, 497, 149–160, https://doi.org/10.1016/j.epsl.2018.06.016, 2018.

Laakso, T. A. and Schrag, D. P.: Methane in the Precambrian atmosphere, Earth and Planetary Science Letters, 522, 48–54, https://doi.org/10.1016/j.epsl.2019.06.022, 2019.

Large, R. R., Mukherjee, I., Gregory, D., Steadman, J., Corkrey, R., and Danyushevsky, L. V.: Atmosphere oxygen cycling through the Proterozoic and Phanerozoic, Mineralium Deposita, 54, 485–506, https://doi.org/10.1007/s00126-019-00873-9, 2019.

Laskar, J., Farhat, M., Lantink, M. L., Auclair-Desrotour, P., Boué, G., and Sinnesael, M.: Did atmospheric thermal tides cause a daylength locking in the Precambrian? A review on recent results, arXiv preprint arXiv:2309.11479, 2023.

Lauro, S. E., Pettinelli, E., Caprarelli, G., Guallini, L., Rossi, A. P., Mattei, E., Cosciotti, B., Cicchetti, A., Soldovieri, F., Cartacci, M., Di Paolo, F., Noschese, R., and Orosei, R.: Multiple subglacial water bodies below the south pole of Mars unveiled by new MARSIS data, Nature Astronomy, 5, 63–70, https://doi.org/10.1038/s41550-020-1200-6, 2021.

Lefèvre, M., Turbet, M., and Pierrehumbert, R.: 3D Convection-resolving Model of Temperate, Tidally Locked Exoplanets, ApJ, 913, 101, https://doi.org/10.3847/1538-4357/abf2c1, 2021.

Lehmer, O. R. and Catling, D. C.: Rocky Worlds Limited to $\sim$1.8 Earth Radii by Atmospheric Escape during a Star's Extreme UV Saturation, ApJ, 845, 130, https://doi.org/10.3847/1538-4357/aa8137, 2017.

Leonovich, L. A. and Tashchilin, A. V.: Variations in ionospheric parameters during solar flares, Geomagnetism and Aeronomy, 49, 983–989, https://doi.org/10.1134/S001679320907024X, 2009.

Lewis, N. T., Lambert, F. H., Boutle, I. A., Mayne, N. J., Manners, J., and Acreman, D. M.: The Influence of a Substellar Continent on the Climate of a Tidally Locked Exoplanet, ApJ, 854, 171, https://doi.org/10.3847/1538-4357/aaad0a, 2018.

Lin, J. and Emanuel, K.: Why the lower stratosphere cools when the troposphere warms, Proceedings of the National Academy of Science, 121, e2319228121, https://doi.org/10.1073/pnas.2319228121, 2024.

Lin, P., Paynter, D., Ming, Y., and Ramaswamy, V.: Changes of the Tropical Tropopause Layer under Global Warming, Journal of Climate, 30, 1245–1258, https://doi.org/10.1175/JCLI-D-16-0457.1, 2017.

Liu, B., Marsh, D. R., Walsh, C., and Cooke, G.: Higher water loss on Earth-like exoplanets in eccentric orbits, MNRAS, 524, 1491–1502, https://doi.org/10.1093/mnras/stad1828, 2023.

Liu, C., Zipser, E., Garrett, T., Jiang, J. H., and Su, H.: How do the water vapor and carbon monoxide "tape recorders" start near the tropical tropopause?, Geophys. Res. Lett., 34, L09804, https://doi.org/10.1029/2006GL029234, 2007.

Liu, H.-L., Bardeen, C. G., Foster, B. T., Lauritzen, P., Liu, J., Lu, G., Marsh, D. R., Maute, A., McInerney, J. M., Pedatella, N. M., Qian, L., Richmond, A. D., Roble, R. G., Solomon, S. C., Vitt, F. M., and Wang, W.: Development and Validation of the Whole Atmosphere Community Climate Model With Thermosphere and Ionosphere Extension (WACCM-X 2.0), Journal of Advances in Modeling Earth Systems, 10, 381–402, https://doi.org/10.1002/2017MS001232, 2018.

Liu, J., Hardisty, D. S., Kasting, J. F., Fakhraee, M., and Planavsky, N. J.: Evolution of the iodine cycle and the late stabilization of the Earth's ozone layer, Proceedings of the National Academy of Sciences, 122, e2412898 121, 2025.

Lovelock, J. E. and Whitfield, M.: Life span of the biosphere, Nature, 296, 561–563, https://doi.org/10.1038/296561a0, 1982.

Lu, J., Xie, F., Tian, H., and Luo, J.: Impacts of Ozone Changes in the Tropopause Layer on Stratospheric Water Vapor, Atmosphere, 12, 291, https://doi.org/10.3390/atmos12030291, 2021.

Lundin, R., Lammer, H., and Ribas, I.: Planetary Magnetic Fields and Solar Forcing: Implications for Atmospheric Evolution, SSRv, 129, 245–278, https://doi.org/10.1007/s11214-007-9176-4, 2007.

Luo, A., Sun, G., Grasby, S. E., and Yin, R.: Large igneous provinces played a major role in oceanic oxygenation events during the mid-Proterozoic, Communications Earth and Environment, 5, 609, https://doi.org/10.1038/s43247-024-01780-2, 2024.

Lyons, T. W., Reinhard, C. T., and Planavsky, N. J.: The rise of oxygen in Earth's early ocean and atmosphere, Nature, 506, 307–315, https://doi.org/10.1038/nature13068, 2014.

Macdonald, E., Paradise, A., Menou, K., and Lee, C.: Climate uncertainties caused by unknown land distribution on habitable M-Earths, MNRAS, 513, 2761–2769, https://doi.org/10.1093/mnras/stac1040, 2022.

Madden, J. and Kaltenegger, L.: How surfaces shape the climate of habitable exoplanets, MNRAS, 495, 1–11, https://doi.org/10.1093/mnras/staa387, 2020.

Maliniemi, V., Nesse Tyssøy, H., Smith-Johnsen, C., Arsenovic, P., and Marsh, D. R.: Effects of enhanced downwelling of NO_x on Antarctic upper-stratospheric ozone in the 21st century, Atmospheric Chemistry & Physics, 21, 11 041–11 052, https://doi.org/10.5194/acp-21-11041-2021, 2021.

Mello, F. d. S. and Friaça, A. C. S.: Planetary geodynamics and age constraints on circumstellar habitable zones around main sequence stars, International Journal of Astrobiology, 22, 272–316, https://doi.org/10.1017/S1473550423000083, 2023.

Mendillo, M.: The ionospheres of planets and exoplanets, Astronomy and Geophysics, 60, 1.25–1.30, https://doi.org/10.1093/astrogeo/atz047, 2019.

Mendillo, M., Withers, P., and Dalba, P. A.: Atomic oxygen ions as ionospheric biomarkers on exoplanets, Nature Astronomy, 2, 287–291, https://doi.org/10.1038/s41550-017-0375-y, 2018.

Mills, B. J. W., Krause, A. J., Jarvis, I., and Cramer, B. D.: Evolution of Atmospheric O_2 Through the Phanerozoic, Revisited, Annual Review of Earth and Planetary Sciences, 51, 253–276, https://doi.org/10.1146/annurev-earth-032320-095425, 2023.

Mitchell, R. N., Zhang, N., Salminen, J., Liu, Y., Spencer, C. J., Steinberger, B., Murphy, J. B., and Li, Z.-X.: The supercontinent cycle, Nature Reviews Earth and Environment, 2, 358–374, https://doi.org/10.1038/s43017-021-00160-0, 2021.

Mote, P. W., Rosenlof, K. H., Holton, J. R., Harwood, R. S., and Waters, J. W.: Seasonal variations of water vapor in the tropical lower stratosphere, Geophys. Res. Lett., 22, 1093–1096, https://doi.org/10.1029/95GL01234, 1995.

Murphy, D. M. and Koop, T.: Review of the vapour pressures of ice and supercooled water for atmospheric applications, Quarterly Journal of the Royal Meteorological Society: A journal of the atmospheric sciences, applied meteorology and physical oceanography, 131, 1539–1565, 2005.

Newell, R. E. and Gould-Stewart, S.: A stratospheric fountain?, Journal of Atmospheric Sciences, 38, 2789–2796, 1981.

Olson, S., Jansen, M. F., Abbot, D. S., Halevy, I., and Goldblatt, C.: The Effect of Ocean Salinity on Climate and Its Implications for Earth's Habitability, Geophys. Res. Lett., 49, e95748, https://doi.org/10.1029/2021GL095748, 2022.

Olson, S. L., Reinhard, C. T., and Lyons, T. W.: Limited role for methane in the mid-Proterozoic greenhouse, Proceedings of the National Academy of Sciences of the United States of America, 113, 11 447–11 452, https://doi.org/10.1073/pnas.1608549113, 2016.

Olson, S. L., Schwieterman, E. W., Reinhard, C. T., and Lyons, T. W.: Earth: Atmospheric Evolution of a Habitable Planet, in: Handbook of Exoplanets, edited by Deeg, H. J. and Belmonte, J. A., p. 189, Springer, https://doi.org/10.1007/978-3-319-55333-7_189, 2018a.

Olson, S. L., Schwieterman, E. W., Reinhard, C. T., Ridgwell, A., Kane, S. R., Meadows, V. S., and Lyons, T. W.: Atmospheric Seasonality as an Exoplanet Biosignature, ApJL, 858, L14, https://doi.org/10.3847/2041-8213/aac171, 2018b.

Orosei, R., Lauro, S. E., Pettinelli, E., Cicchetti, A., Coradini, M., Cosciotti, B., Di Paolo, F., Flamini, E., Mattei, E., Pajola, M., Soldovieri, F., Cartacci, M., Cassenti, F., Frigeri, A., Giuppi, S., Martufi, R., Masdea, A., Mitri, G., Nenna, C., Noschese, R., Restano, M., and Seu, R.: Radar evidence of subglacial liquid water on Mars, Science, 361, 490–493, https://doi.org/10.1126/science.aar7268, 2018.

Owen, J. E. and Alvarez, M. A.: UV Driven Evaporation of Close-in Planets: Energy-limited, Recombination-limited, and Photon-limited Flows, ApJ, 816, 34, https://doi.org/10.3847/0004-637X/816/1/34, 2016.

Ozaki, K. and Reinhard, C. T.: The future lifespan of Earth's oxygenated atmosphere, Nature Geoscience, 14, 138–142, https://doi.org/10.1038/s41561-021-00693-5, 2021.

Paulik, L. C. and Birner, T.: Quantifying the deep convective temperature signal within the tropical tropopause layer (TTL), Atmospheric Chemistry & Physics, 12, 12 183–12 195, https://doi.org/10.5194/acp-12-12183-201210.5194/acpd-12-19617-2012, 2012.

Pavlov, A. A., Hurtgen, M. T., Kasting, J. F., and Arthur, M. A.: Methane-rich Proterozoic atmosphere?, Geology, 31, 87, https://doi.org/10.1130/0091-7613(2003)031<0087:MRPA>2.0.CO;2, 2003.

Pilch Kedzierski, R., Matthes, K., and Bumke, K.: The tropical tropopause inversion layer: variability and modulation by equatorial waves, Atmospheric Chemistry and Physics, 16, 11 617–11 633, 2016.

Planavsky, N. J., Reinhard, C. T., Isson, T. T., Ozaki, K., and Crockford, P. W.: Large Mass-Independent Oxygen Isotope Fractionations in Mid-Proterozoic Sediments: Evidence for a Low-Oxygen Atmosphere?, Astrobiology, 20, 628–636, https://doi.org/10.1089/ast.2019.2060, 2020.

Pommereau, J. P. and Held, G.: Is there a stratospheric fountain?, Atmospheric Chemistry & Physics Discussions, 7, 8933–8950, https://doi.org/10.5194/acpd-7-8933-2007, 2007.

Pope, E. C., Bird, D. K., and Rosing, M. T.: Isotope composition and volume of Earth's early oceans, Proceedings of the National Academy of Science, 109, 4371–4376, https://doi.org/10.1073/pnas.1115705109, 2012.

Pumphrey, H. C., Boone, C., Walker, K. A., Bernath, P., and Livesey, N. J.: Tropical tape recorder observed in HCN, Geophys. Res. Lett., 35, L05801, https://doi.org/10.1029/2007GL032137, 2008.

Randel, W. J. and Jensen, E. J.: Physical processes in the tropical tropopause layer and their roles in a changing climate, Nature Geoscience, 6, 169–176, https://doi.org/10.1038/ngeo1733, 2013.

Ridgway, R. J., Zamyatina, M., Mayne, N. J., Manners, J., Lambert, F. H., Braam, M., Drummond, B., Hébrard, E., Palmer, P. I., and Kohary, K.: 3D modelling of the impact of stellar activity on tidally locked terrestrial exoplanets: atmospheric composition and habitability, MNRAS, 518, 2472–2496, https://doi.org/10.1093/mnras/stac3105, 2023.

Rogers, J. J. W. and Santosh, M.: Configuration of Columbia, a Mesoproterozoic Supercontinent, Gondwana Research, 5, 5–22, https://doi.org/10.1016/S1342-937X(05)70883-2, 2002.

Rosenfield, J. E., Douglass, A. R., and Considine, D. B.: The impact of increasing carbon dioxide on ozone recovery, Journal of Geophysical Research (Atmospheres), 107, 4049, https://doi.org/10.1029/2001JD000824, 2002.

Rugheimer, S. and Kaltenegger, L.: Spectra of Earth-like Planets through Geological Evolution around FGKM Stars, ApJ, 854, 19, https://doi.org/10.3847/1538-4357/aaa47a, 2018.

Rugheimer, S., Segura, A., Kaltenegger, L., and Sasselov, D.: UV Surface Environment of Earth-like Planets Orbiting FGKM Stars through Geological Evolution, ApJ, 806, 137, https://doi.org/10.1088/0004-637X/806/1/137, 2015.

Rushby, A. J., Johnson, M., Mills, B. J. W., Watson, A. J., and Claire, M. W.: Long-Term Planetary Habitability and the Carbonate-Silicate Cycle, Astrobiology, 18, 469–480, https://doi.org/10.1089/ast.2017.1693, 2018.

Salz, M., Schneider, P. C., Czesla, S., and Schmitt, J. H. M. M.: Energy-limited escape revised. The transition from strong planetary winds to stable thermospheres, A&A, 585, L2, https://doi.org/10.1051/0004-6361/201527042, 2016.

Sandu, A., Verwer, J., Van Loon, M., Carmichael, G., Potra, F., Dabdub, D., and Seinfeld, J.: Benchmarking stiff ode solvers for atmospheric chemistry problems-I. implicit vs explicit, Atmospheric environment, 31, 3151–3166, 1997.

Saunois, M., Martinez, A., Poulter, B., Zhang, Z., Raymond, P. A., Regnier, P., Canadell, J. G., Jackson, R. B., Patra, P. K., Bousquet, P., Ciais, P., Dlugokencky, E. J., Lan, X., Allen, G. H., Bastviken, D., Beerling, D. J., Belikov, D. A., Blake, D. R., Castaldi, S., Crippa, M., Deemer, B. R., Dennison, F., Etiope, G., Gedney, N., Höglund-Isaksson, L., Holgerson, M. A., Hopcroft, P. O., Hugelius, G., Ito, A., Jain, A. K., Janardanan, R., Johnson, M. S., Kleinen, T., Krummel, P. B., Lauerwald, R., Li, T., Liu, X., McDonald, K. C., Melton, J. R., Mühle, J., Müller, J., Murguia-Flores, F., Niwa, Y., Noce, S., Pan, S., Parker, R. J., Peng, C., Ramonet, M., Riley, W. J., Rocher-Ros, G., Rosentreter, J. A., Sasakawa, M., Segers, A., Smith, S. J., Stanley, E. H., Thanwerdas, J., Tian, H., Tsuruta, A., Tubiello, F. N., Weber,

T. S., van der Werf, G. R., Worthy, D. E. J., Xi, Y., Yoshida, Y., Zhang, W., Zheng, B., Zhu, Q., Zhu, Q., and Zhuang, Q.: Global Methane Budget 2000-2020, Earth System Science Data, 17, 1873–1958, https://doi.org/10.5194/essd-17-1873-2025, 2025.

Sauterey, B., Charnay, B., Affholder, A., Mazevet, S., and Ferrière, R.: Early Mars habitability and global cooling by H_2-based methanogens, Nature Astronomy, 6, 1263–1271, https://doi.org/10.1038/s41550-022-01786-w, 2022.

Scheller, E. L., Ehlmann, B. L., Hu, R., Adams, D. J., and Yung, Y. L.: Long-term drying of Mars by sequestration of ocean-scale volumes of water in the crust, Science, 372, 56–62, https://doi.org/10.1126/science.abc7717, 2021.

Schillings, A., Nilsson, H., Slapak, R., Wintoft, P., Yamauchi, M., Wik, M., Dandouras, I., and Carr, C. M.: O^+ Escape During the Extreme Space Weather Event of 4-10 September 2017, Space Weather, 16, 1363–1376, https://doi.org/10.1029/2018SW001881, 2018.

Schoeberl, M. R., Duncan, B. N., Douglass, A. R., Waters, J., Livesey, N., Read, W., and Filipiak, M.: The carbon monoxide tape recorder, Geophys. Res. Lett., 33, L12811, https://doi.org/10.1029/2006GL026178, 2006.

Schulik, M. and Booth, R. A.: AIOLOS - A multipurpose 1D hydrodynamics code for planetary atmospheres, MNRAS, 523, 286–304, https://doi.org/10.1093/mnras/stad1251, 2023.

Segura, A., Krelove, K., Kasting, J. F., Sommerlatt, D., Meadows, V., Crisp, D., Cohen, M., and Mlawer, E.: Ozone Concentrations and Ultraviolet Fluxes on Earth-Like Planets Around Other Stars, Astrobiology, 3, 689–708, https://doi.org/10.1089/153110703322736024, 2003.

Segura, A., Meadows, V. S., Kasting, J. F., Crisp, D., and Cohen, M.: Abiotic formation of O_2 and O_3 in high-CO_2 terrestrial atmospheres, A&A, 472, 665–679, https://doi.org/10.1051/0004-6361:20066663, 2007.

Segura, A., Walkowicz, L. M., Meadows, V., Kasting, J., and Hawley, S.: The Effect of a Strong Stellar Flare on the Atmospheric Chemistry of an Earth-like Planet Orbiting an M Dwarf, Astrobiology, 10, 751–771, https://doi.org/10.1089/ast.2009.0376, 2010.

Sergeev, D. E., Lambert, F. H., Mayne, N. J., Boutle, I. A., Manners, J., and Kohary, K.: Atmospheric Convection Plays a Key Role in the Climate of Tidally Locked Terrestrial Exoplanets: Insights from High-resolution Simulations, ApJ, 894, 84, https://doi.org/10.3847/1538-4357/ab8882, 2020.

Sergeev, D. E., Mayne, N. J., Bendall, T., Boutle, I. A., Brown, A., Kavčič, I., Kent, J., Kohary, K., Manners, J., Melvin, T., Olivier, E., Ragta, L. K., Shipway, B., Wakelin, J., Wood, N., and Zerroukat, M.: Simulations of idealised 3D atmospheric flows on terrestrial planets using LFRic-Atmosphere, Geoscientific Model Development, 16, 5601–5626, https://doi.org/10.5194/gmd-16-5601-2023, 2023.

Sergeev, D. E., Boutle, I. A., Lambert, F. H., Mayne, N. J., Bendall, T., Kohary, K., Olivier, E., and Shipway, B.: The Impact of the Explicit Representation of Convection on the Climate of a Tidally Locked Planet in Global Stretched-mesh Simulations, ApJ, 970, 7, https://doi.org/10.3847/1538-4357/ad4ecd, 2024.

Sheldon, N. D.: Precambrian paleosols and atmospheric CO2 levels, Precambrian Research, 147, 148–155, https://doi.org/10.1016/j.precamres.2006.02.004, 2006.

Sheldon, N. D.: Causes and consequences of low atmospheric pCO2 in the Late Mesoproterozoic, Chemical Geology, 362, 224–231, https://doi.org/10.1016/j.chemgeo.2013.09.006, 2013.

Shematovich, V. I. and Marov, M. Y.: Escape of planetary atmospheres: physical processes and numerical models, Physics Uspekhi, 61, 217, https://doi.org/10.3367/UFNe.2017.09.038212, 2018.

Song, Q., Yang, J., Luo, H., Li, C., and Fu, S.: Idealized 2D Cloud-resolving Simulations for Tidally Locked Habitable Planets, ApJ, 934, 149, https://doi.org/10.3847/1538-4357/ac7879, 2022.

Steadman, J. A., Large, R. R., Blamey, N. J., Mukherjee, I., Corkrey, R., Danyushevsky, L. V., Maslennikov, V., Hollings, P., Garven, G., Brand, U., and Lécuyer, C.: Evidence for elevated and variable atmospheric oxygen in the Precambrian, Precambrian Research, 343, 105 722, https://doi.org/10.1016/j.precamres.2020.105722, 2020.

Stockey, R. G., Cole, D. B., Farrell, U. C., Agić, H., Boag, T. H., Brocks, J. J., Canfield, D. E., Cheng, M., Crockford, P. W., Cui, H., Dahl, T. W., Del Mouro, L., Dewing, K., Dornbos, S. Q., Emmings, J. F., Gaines, R. R., Gibson, T. M., Gill, B. C., Gilleaudeau, G. J., Goldberg, K., Guilbaud, R., Halverson, G., Hammarlund, E. U., Hantsoo, K., Henderson, M. A., Henderson, C. M., Hodgskiss, M. S. W., Jarrett, A. J. M., Johnston, D. T., Kabanov, P., Kimmig, J., Knoll, A. H., Kunzmann, M., LeRoy, M. A., Li, C., Loydell, D. K., Macdonald, F. A., Magnall, J. M., Mills, N. T., Och, L. M., O'Connell, B., Pagès, A., Peters, S. E., Porter, S. M., Poulton, S. W., Ritzer, S. R., Rooney, A. D., Schoepfer, S., Smith, E. F., Strauss, J. V., Uhlein, G. J., White, T., Wood, R. A., Woltz, C. R., Yurchenko, I., Planavsky, N. J., and Sperling, E. A.: Sustained increases in atmospheric oxygen and marine productivity in the Neoproterozoic and Palaeozoic eras, Nature Geoscience, 17, 667–674, https://doi.org/10.1038/s41561-024-01479-1, 2024.

Tegtmeier, S., Anstey, J., Davis, S., Ivanciu, I., Jia, Y., McPhee, D., and Pilch Kedzierski, R.: Zonal Asymmetry of the QBO Temperature Signal in the Tropical Tropopause Region, Geophys. Res. Lett., 47, e89533, https://doi.org/10.1029/2020GL089533, 2020.

Tian, F., Toon, O. B., Pavlov, A. A., and De Sterck, H.: A Hydrogen-Rich Early Earth Atmosphere, Science, 308, 1014–1017, https://doi.org/10.1126/science.1106983, 2005.

Tilley, M. A., Segura, A., Meadows, V., Hawley, S., and Davenport, J.: Modeling Repeated M Dwarf Flaring at an Earth-like Planet in the Habitable Zone: Atmospheric Effects for an Unmagnetized Planet, Astrobiology, 19, 64–86, https://doi.org/10.1089/ast.2017.1794, 2019.

Turbet, M., Leconte, J., Selsis, F., Bolmont, E., Forget, F., Ribas, I., Raymond, S. N., and Anglada-Escudé, G.: The habitability of Proxima Centauri b. II. Possible climates and observability, A&A, 596, A112, https://doi.org/10.1051/0004-6361/201629577, 2016.

Turbet, M., Bolmont, E., Chaverot, G., Ehrenreich, D., Leconte, J., and Marcq, E.: Day-night cloud asymmetry prevents early oceans on Venus but not on Earth, Nature, 598, 276–280, https://doi.org/10.1038/s41586-021-03873-w, 2021.

Von Bloh, W., Franck, S., Bounama, C., and Schellnhuber, H.-J.: Biogenic enhancement of weathering and the stability of the ecosphere, Geomicrobiology Journal, 20, 501–511, 2003.

Walker, J. C. G.: Evolution of the atmosphere, Macmillan, 1977.

Wang, T. and Dessler, A. E.: Analysis of cirrus in the tropical tropopause layer from CALIPSO and MLS data: A water perspective, Journal of Geophysical Research (Atmospheres), 117, D04211, https://doi.org/10.1029/2011JD016442, 2012.

Warke, M. R., Di Rocco, T., Zerkle, A. L., Lepland, A., Prave, A. R., Martin, A. P., Ueno, Y., Condon, D. J., and Claire, M. W.: The Great Oxidation Event preceded a Paleoproterozoic "snowball Earth", Proceedings of the National Academy of Science, 117, 13 314–13 320, https://doi.org/10.1073/pnas.2003090117, 2020.

Warren, A. O. and Kite, E. S.: Narrow range of early habitable Venus scenarios permitted by modeling of oxygen loss and radiogenic argon degassing, Proceedings of the National Academy of Science, 120, e2209751120, https://doi.org/10.1073/pnas.2209751120, 2023.

Way, M. J., Aleinov, I., Amundsen, D. S., Chandler, M. A., Clune, T. L., Del Genio, A. D., Fujii, Y., Kelley, M., Kiang, N. Y., Sohl, L., and Tsigaridis, K.: Resolving Orbital and Climate Keys of Earth and Extraterrestrial Environments with Dynamics (ROCKE-3D) 1.0: A General Circulation Model for Simulating the Climates of Rocky Planets, ApJS, 231, 12, https://doi.org/10.3847/1538-4365/aa7a06, 2017.

Wolf, E. T. and Toon, O. B.: Delayed onset of runaway and moist greenhouse climates for Earth, Geophys. Res. Lett., 41, 167–172, https://doi.org/10.1002/2013GL058376, 2014.

Wordsworth, R. and Pierrehumbert, R.: Abiotic Oxygen-dominated Atmospheres on Terrestrial Habitable Zone Planets, ApJL, 785, L20, https://doi.org/10.1088/2041-8205/785/2/L20, 2014.

Wright, V., Morzfeld, M., and Manga, M.: Liquid water in the Martian mid-crust, Proceedings of the National Academy of Sciences, 121, e2409983 121, 2024.

Xie, B., Zhu, J.-m., Wang, X., Xu, D., Zhou, L., Zhou, X., Shi, X., and Tang, D.: Mesoproterozoic oxygenation event: From shallow marine to atmosphere, Geological Society of America Bulletin, 135, 753–766, https://doi.org/10.1130/B36407.1, 2023.

Xie, F., Tian, W., and Chipperfield, M. P.: Radiative effect of ozone change on stratosphere-troposphere exchange, Journal of Geophysical Research (Atmospheres), 113, D00B09, https://doi.org/10.1029/2008JD009829, 2008.

Yang, J., Zhang, Y., Fu, Z., Yan, M., Song, X., Wei, M., Liu, J., Ding, F., and Tan, Z.: Cloud behaviour on tidally locked rocky planets from global high-resolution modelling, Nature Astronomy, 7, 1070–1080, https://doi.org/10.1038/s41550-023-02015-8, 2023.

Yassin Jaziri, A., Charnay, B., Selsis, F., Leconte, J., and Lefèvre, F.: Dynamics of the Great Oxidation Event from a 3D photochemical-climate model, Climate of the Past, 18, 2421–2447, https://doi.org/10.5194/cp-18-2421-2022, 2022.

Yierpan, A., König, S., Labidi, J., and Schoenberg, R.: Recycled selenium in hot spot–influenced lavas records ocean-atmosphere oxygenation, Science Advances, 6, eabb6179, 2020.

Young, G. M.: Precambrian supercontinents, glaciations, atmospheric oxygenation, metazoan evolution and an impact that may have changed the second half of Earth history, Geoscience Frontiers, 4, 247–261, 2013.

Zahnle, K. and Walker, J. C. G.: A constant daylength during the precambrian era?, Precambrian Research, 37, 95–105, https://doi.org/10.1016/0301-9268(87)90073-8, 1987.

Zahnle, K. J., Catling, D. C., and Claire, M. W.: The rise of oxygen and the hydrogen hourglass, Chemical Geology, 362, 26–34, https://doi.org/10.1016/j.chemgeo.2013.08.004, 2013.

Zahnle, K. J., Gacesa, M., and Catling, D. C.: Strange messenger: A new history of hydrogen on Earth, as told by Xenon, GeoCoA, 244, 56–85, https://doi.org/10.1016/j.gca.2018.09.017, 2019.

Zhao, M., Reinhard, C. T., and Planavsky, N.: Terrestrial methane fluxes and Proterozoic climate, Geology, 46, 139–142, https://doi.org/10.1130/G39502.1, 2018.

Zhao, M., Reinhard, C. T., and Planavsky, N.: Terrestrial methane fluxes and Proterozoic climate, Geology, 46, 139–142, 2018.

Zhao, Z., Liu, Y., Li, W., Liu, H., and Man, K.: Climate Change of over 20 °C Induced by Continental Movement on a Synchronously Rotating Exoplanet, ApJL, 910, L8, https://doi.org/10.3847/2041-8213/abebe6, 2021.

Zheng, N., Ding, C., Su, Y., and Orosei, R.: Water Ice Resources on the Shallow Subsurface of Mars: Indications to Rover-Mounted Radar Observation, Remote Sensing, 16, 824, https://doi.org/10.3390/rs16050824, 2024.

Zhou, L., Xia, Y., and Zhao, C.: Influence of Stratospheric Ozone Changes on Stratospheric Temperature Trends in Recent Decades, Remote Sensing, 14, 5364, https://doi.org/10.3390/rs14215364, 2022.

Zhu, Q., Jung, D. Y., Oganov, A. R., Glass, C. W., Gatti, C., and Lyakhov, A. O.: Stability of xenon oxides at high pressures, Nature Chemistry, 5, 61–65, https://doi.org/10.1038/nchem.1497, 2013.

Zilinskas, M., Miguel, Y., Lyu, Y., and Bax, M.: Temperature inversions on hot super-Earths: the case of CN in nitrogen-rich atmospheres, MNRAS, 500, 2197–2208, https://doi.org/10.1093/mnras/staa3415, 2021.

Zolghadrshojaee, M., Tegtmeier, S., Davis, S. M., and Pilch Kedzierski, R.: Variability And Long-Term Changes In Tropical Cold-Point Temperature And Water Vapor, Atmospheric Chemistry & Physics, 24, 7405–7419, https://doi.org/10.5194/acp-24-7405-2024, 2024.

Zou, L., Hoffmann, L., Müller, R., and Spang, R.: Variability and trends of the tropical tropopause derived from a 1980–2021 multi-reanalysis assessment, Frontiers in Earth Science, 11, 1177502, https://doi.org/10.3389/feart.2023.1177502, 2023.